Deciphering an Undecided Enzyme: Investigations of the Structural Determinants Involved in the Linkage Specificity of Alternansucrase

Manon Molina, Claire Moulis, Nelly Monties, Sandra Pizzut-Serin, David Guieysse, Sandrine Morel, Gianluca Cioci, Magali Remaud-Siméon

ACS Catalysis

Research Article

Cite This: ACS Catal. 2019, 9, 2222−2237

pubs.acs.org/acscatalysis

Deciphering an Undecided Enzyme: Investigations of the Structural Determinants Involved in the Linkage Specificity of Alternansucrase

Manon Molina, Claire Moulis, Nelly Monties, Sandra Pizzut-Serin, David Guieysse, Sandrine Morel, Gianluca Cioci,* and Magali Remaud-Siméon*

LISBP (Laboratoire d'Ingénierie des Systèmes Biologiques et des Procédés), Université de Toulouse, CNRS (Centre National de la Recherche Scientifique), INRA (Institut National de la Recherche Agronomique), INSA (Institut National des Sciences Appliquées), F-31077 Toulouse, France

Supporting Information

ABSTRACT: Understanding how polymerases catalyze the synthesis of biopolymers is a timely and important issue in generating controlled structures with well-defined properties. With this objective in mind, here we describe the 2.8 Å crystal structure of a truncated version of alternansucrase (ASR) from *L. citreum* NRRL B-1355. Indeed, ASR is a striking example of α-transglucosylase among GH70 glucansucrases, capable of catalyzing high and low molar mass alternan, an α-glucan comprising alternating α-1,3 and α-1,6 linkages in its linear chain. The 3D structure sheds light on the various features involved in enzyme stability. Moreover, docking studies and biochemical characterizations of 17 single mutants and two double mutants enable the key determinants of α-1,6 or α-1,3 linkage specificity to be located and establish the structural basis of alternance. ASR displays two different acceptor subsites in the prolongation of its subsites −1 and +1. The first one is defined by Trp675, a residue of subsite +2, and orients acceptor binding exclusively toward α-1,6 linkage synthesis. The second binding site comprises Asp772 and Trp543, two residues defining the +2′ and +3′ subsites, respectively, which are critical for α-1,3 linkage formation. It is proposed that the interplay between these two acceptor sites controls alternance. These results add to the toolbox of enzymes for the production of tailor-made polysaccharides with controlled structures.

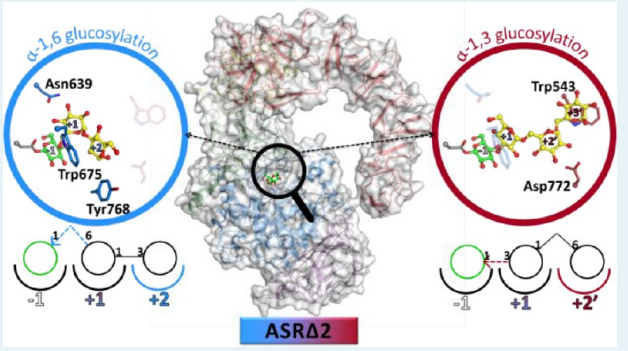

KEYWORDS: *glucansucrase, alternansucrase, alternan, crystal structure, GH70, α-(1→3)/α-(1→6) linkage specificity and alternance*

INTRODUCTION

The α-glucans constitute an important class of polymers, among which those produced using glucansucrases (GSs) from the GH70 family are particularly attractive for applications in medicine, nutrition, cosmetics, and materials science.[1−4] They are synthesized directly from sucrose, an abundant substrate available in a highly pure form. A broad variety of molecular structures can be easily obtained depending on the enzymes involved in their synthesis. Indeed, the size, type, and arrangement of α-osidic linkages as well as the degree of branching can vary considerably from one polymer to another. All of these factors define the physicochemical, biological, and mechanical properties of each specimen and therefore its range of application. Improving the understanding of the molecular features at the origin of glucansucrase specificity and diversity is therefore essential for further development of α-glucans with tightly controlled structures.

In an impressive study aiming to characterize the polysaccharides produced by almost 100 different lactic acid bacteria, Jeanes et al. were the first to report the presence of an α-glucan containing alternating α-1,3 and α-1,6 osidic linkages in the culture supernatant of several strains of *Leuconostoc* sp., such as *L. mesenteroides* NRRL B-1355 (recently reclassified as *L. citreum*[5]), NRRL B-1501, and NRRL B-1498.[6] Different analytical techniques (periodate oxidation, methylation, acetolysis, Smith reaction, NMR, and enzymatic digestion) confirmed the presence of around 40% α-1,3 linkages and 60% α-1,6 linkages in the polymer (as determined by NMR on purified alternan), with the occurrence of alternating α-1,3 and α-1,6 linkages in the polymer chain, as well as some consecutive α-1,6 linkages and around 10% branching linkages.[6−19] The polymer was named alternan. The enzymatic activity responsible for its synthesis was isolated and referred to as alternansucrase (ASR, EC 2.4.1.140).[7] With an optimum temperature of 45 °C, ASR is one of the most stable enzymes in the GH70 family, which enabled the enzyme to be purified using a thermal treatment.[20,21] Further, the *asr* gene from *L. citreum* NRRL B-1355 was expressed in *E. coli*.[22] The

Received: November 9, 2018
Revised: January 22, 2019
Published: January 29, 2019

DOI: 10.1021/acscatal.8b04510
ACS Catal. 2019, 9, 2222−2237

recombinant protein was shown to produce, from sucrose, a bimodal population of glucan, comprising a high molar mass (HMM) fraction of 1 700 000 g·mol^{-1} as estimated by size exclusion chromatography and a low molar mass (LMM) fraction of 1300 g·mol^{-1}.[11] Sequences sharing more than 97% identity with *L. citreum* NRRL B-1355 ASR sequence are found at present in the genome of other *L. citreum* strains (LBAE C11, KM20, EFEL 2700, ABK-1), suggesting that ASR is widespread in these species (BLASTp analysis, data not shown). To date, only one other alternansucrase from *L. citreum* ABK-1 has been produced recombinantly and characterized.[23]

Alternan polymer is more water soluble and less viscous than dextrans, making it a good substitute for Arabic gum.[12,24] Nanoparticles and films were recently obtained with alternan produced by *L. citreum* ABK-1 alternansucrase, thereby opening up other potential applications in nanotechnology.[23] Moreover, ASR also catalyzes transglucosylation from sucrose to many different types of sugar acceptors—methyl-α-D-glucoside, maltose, maltodextrin, maltitol, isomaltooligosaccharides,[20] cellobiose,[25] melibiose, raffinose, gentiobiose, and lactose—and produces glucosylated products showing interesting prebiotic properties.[26−28] Stevioside-glucosides showing promising noncariogenic and low-calorie properties were also synthesized.[29] Finally, ASR was also recently used to elongate amylose chains of DP 30 and create a linker between amylose and linear dextran, enabling the production of a triblock polymer using enzymatic technologies alone.[30]

Sequence analysis revealed that ASR belongs to the GH70 family. The enzyme was predicted to adopt the same fold as the other glucansucrases and the same α-retaining mechanism involving the contribution of Asp635, Glu673, and Asp767. It was suggested that these amino acids play the role of, respectively, the nucleophile, acid/base catalyst, and transition state stabilizer (TSS) implicated in the formation of the β-D-glucosyl−enzyme intermediate.[22] Unusual repeated sequences named "APY repeats" were identified at the C-terminal end of the protein.[31] Their deletion in the mutant ASR C-APY-del (covering amino acids Met1 to Gly1425) did not impact the product profile[11] but significantly increased (5-fold) the enzyme half-life time at 50 °C compared to the entire ASR.[32] A kinetic study conducted with ASR C-APY-del showed that both HMM and LMM alternan populations are formed in the early stage of the reaction, suggesting that ASR follows a semiprocessive mechanism of polymerization.[14] In addition, a mutagenesis study of ASR C-APY-del highlighted the importance of the triplet ^{768}YDA^{770} (downstream of the putative TSS stabilizer Asp767 and found solely in ASR) in linkage specificity.[14] Replacement of this motif with the triplet SEV, which is characteristic of glucansucrase and highly specific to α-1,6 linkage synthesis, resulted in a variant synthesizing both oligoalternans and oligodextrans up to a degree of polymerization 4 (DP4) through successive glucosylations of the maltose acceptor. However, contrary to the wild-type ASR, the mutant was unable to further elongate the DP4 oligoalternan, which resulted in its accumulation. Only the oligodextrans were further elongated via α-1,6 linkage synthesis.

Despite the multiple attributes of alternansucrase from *L. citreum* NRRL B-1355—namely, (i) its thermal stability, (ii) its potential for the production of prebiotic compounds, glycoconjugates and new biomaterials, and (iii) the very unique specificity of this glucansucrase for alternating α-1,3 and α-1,6 linkage synthesis—information related to the structural determinants impacting linkage specificity and stability remains scarce. Here, we explore further the structure−function relationships of this enzyme and disclose the first X-ray three-dimensional structure of a GH70 alternansucrase. With 1278 residues, the new free 3D structure of ASRΔ2 was obtained at 2.8 Å resolution. It is the largest GH70 enzyme structure solved so far. Structural analysis combined with mutagenesis studies and biochemical characterization enabled the identification of different features and amino acids exerting a critical role in stability, specificity, and ratio of LMM to HMM polymers.

EXPERIMENTAL PROCEDURES

Truncated Mutant Design and Construction. SignalP,[33] DisEMBL,[34] RONN,[35] and PSIPRED[36] web servers were used to design N-terminal truncations.

Genes of *asr*-Δ2, *asr*-Δ3, *asr*-Δ4, and *asr*-Δ5 were amplified by PCR using the *asr*-Cdel gene as a template, Phusion polymerase (NEB), and the following primers: *asr*-Δ2 forward primer CAC-CGC-GGA-TAC-AAA-TTC-G, *asr*-Δ3 forward primer CAC-CGG-TTT-TTG-GTA-TGA-TTC-AG, *asr*-Δ4 forward primer CAC-CAT-CAC-TGG-GGG-TCA-C, *asr*-Δ2/Δ3/Δ4 reverse primer CCC-TCG-AGA-CAT-AGT-CCC-ATC, *asr*-Δ5 forward primer CAC−CCA-AAG-TAA-TGA-AAA-TAC-TCC, and *asr*-Δ5 reverse primer CGC-ATC-TTT-ATT-CTG-CAA-CTG. A "CACC" sequence was added at the beginning of each forward primer for cloning in pENTR D-TOPO vector before being recombined in pET53-DEST vector (Gateway system, Thermo Fisher Scientific). The recombined product was transformed into competent *E. coli* TOP10 (Invitrogen). Each gene in the pENTR plasmid was verified by sequencing (GATC Biotech).

Production and Purification of Truncated Enzymes. The *E. coli* BL21 DE3* strain was used for enzyme production. A preculture of transformed *E. coli* BL21 DE3* in LB medium supplemented with ampicillin 100 μg·mL^{-1} was used to inoculate a culture at an $OD_{600\ nm}$ of 0.05 in ZYM-5052 autoinducible medium[37] modified by supplementation with 100 μg·mL^{-1} ampicillin, 1% (w/v) α-lactose, and 1% (w/v) glycerol for pET53 enzyme production. After 26 h of growing at 21 °C, cells were harvested by centrifugation and resuspended in binding buffer containing 20 mM phosphate buffer, 20 mM imidazole (Merck Millipore), and 500 mM NaCl, pH 7.4 supplemented with EDTA-free antiprotease tablets (Roche). Cells were disrupted by sonication, and debris was removed by a centrifugation step at 45 000*g* for 30 min at 8 °C. Purification was performed with the ÄKTA Xpress system (GE Healthcare). Two-step purification was performed in a cold chamber at 8 °C using (i) a HisTrap HP 1 mL column (GE Healthcare) for the affinity step and (ii) a Superose12 16/60 (GE Healthcare) for the size exclusion step or a HiPrep desalting 26/10 column (GE Healthcare) for desalting. The size exclusion step was performed upstream of crystallization trials and differential scanning fluorimetry assays, and protein was eluted in MES buffer pH 6.5 at 30 mM with 100 mM NaCl and 0.05 g·L^{-1} $CaCl_2$. The desalting step was performed for biochemical characterization, for which protein was eluted in 50 mM sodium acetate buffer pH 5.75. Purified fractions were pooled together and concentrated using AmiconUltra-15 with a cutoff of 50 kDa to 10−15 mg·mL^{-1}. Purification was checked by SDS-Page electrophoresis using NuPAGE 3−8% Tris-Acetate protein gels (Invitrogen), and

DOI: 10.1021/acscatal.8b04510
ACS Catal. 2019, 9, 2222−2237

protein concentration was assessed by spectroscopy at 280 nm using a NanoDrop instrument. The theoretical molecular weight and molar extinction coefficient of the enzyme were calculated using the ExPASy ProtParam tool (https://web.expasy.org/protparam/).

Mutagenesis Study. Mutants were constructed by inverse PCR using the pET53-*asr*-Δ2 gene as a template, Phusion polymerase (NEB), and the primers described in Table S1. Following overnight *Dpn*I (NEB) digestion, the PCR product was transformed into competent *E. coli* DH5α and clones were selected on solid LB medium supplemented with ampicillin 100 $\mu g \cdot mL^{-1}$. Plasmids were extracted with the QIAGEN spin miniprep kit, and mutated *asr* genes were checked by sequencing (GATC Biotech). Mutants were produced and purified as described above.

Activity Measurement. Activity was determined in triplicate at 30 °C in a Thermomixer (Eppendorf) using the 3,5-dinitrosalicylic acid method.[38] Fifty millimolar sodium acetate buffer pH 5.75, 292 mM sucrose, and 0.05 $mg \cdot mL^{-1}$ of pure enzyme were used. One unit of activity is defined as the amount of enzyme that hydrolyzes 1 μmol of sucrose per minute. To evaluate the calcium effect, initial activity was measured with 3.4 mM calcium chloride, 5 mM EDTA, or without additives under the same conditions as above.

Enzymatic Reactions and Product Characterization. Polymer productions were performed using 1 $U \cdot mL^{-1}$ of pure enzyme with 292 mM sucrose in 50 mM NaAc buffer pH 5.75 at 30 °C over a period of 24 h. The products were analyzed using high-pressure size exclusion chromatography (HPSEC) with Shodex OH-Pak 805 and 802.5 columns in series in a 70 °C oven with a flow rate of 0.250 $mL \cdot min^{-1}$ connected to a RI detector. The eluent was 50 mM sodium acetate, 0.45 M sodium nitrate, and 1% (v/v) ethylene glycol. The ratios of HMM polymer to LMM polymer produced were calculated using the area of each peak divided by the sum of the areas. The same sample was analyzed in triplicate in HPSEC.

Acceptor reactions were set up in the presence of maltose (sucrose:maltose mass ratio 2:1) in the same conditions. The products were analyzed by high-pressure anion exchange chromatography with pulsed amperometric detection (HPAEC-PAD) using a CarboPac TM PA100 guard column upstream of a CarboPac TM PA100 analytical column (2 mm × 250 mm) at a flow rate of 0.250 $mL \cdot min^{-1}$. The eluents were A = 150 mM NaOH and B = 500 mM sodium acetate with 150 mM NaOH. Sugars were eluted with an increasing 0−60% gradient of eluent B for 30 min. Quantification was performed using standards of glucose and sucrose at 5, 10, 15, and 20 $mg \cdot L^{-1}$. The hydrolysis percentage was calculated by dividing the final molar concentration of glucose by the initial molar concentration of sucrose. The degree of polymerization (DP) of the oligosaccharides produced was determined using HPAEC coupled with a simple quadrupole mass spectrometer (ISQ EC, Thermo Scientific), and sugars were eluted under the same conditions as above with a 0−30% gradient of eluent B for 45 min. A mass spectrometer fitted with an ESI ion source was used with the following parameters: collision-induced dissociation (CID) of 10 V, vaporizer temperature of 289 °C, ion transfer tube temperature of 300 °C, and source voltage of 3 kV in positive mode. The mass spectrometry range was m/z 100−1250 (maximum DP 7). To identify the peaks, an acceptor reaction was set up under the same conditions as above with the dextransucrase DSR-S vardel Δ4N, which elongates maltose only through α-1,6 linkages. These peaks correspond to oligodextran (OD) and only contain linear α-1,6 linkages joined to maltose. The ASRΔ2 and DSR-S vardel Δ4N oligosaccharides were coeluted to ensure peak attribution (Figure S1). The other main oligosaccharides obtained with the ASRΔ2 reaction from maltose were named oligoalternan (OA) of DP3−6. Oligoalternans contain both α-1,6 and α-1,3 linkages, and their structure is well defined in the literature.[20,39,40]

NMR samples were prepared by dissolving 10 mg of the total products from sucrose in 0.5 mL of D_2O. Deuterium oxide was used as the solvent, and sodium 2,2,3,3-tetradeuterio-3-trimethylsilylpropanoate ($TSPD_4$) was selected as the internal standard (δ^1H = 0 ppm, $\delta^{13}C$ = 0 ppm). ^1H and ^{13}C NMR spectra were recorded on a Bruker Avance 500-MHz spectrometer operating at 500.13 MHz for ^1H NMR and 125.75 MHz for ^{13}C using a 5 mm z-gradient TBI probe. The data were processed using TopSpin 3.0 software. 1D ^1H NMR spectra were acquired by using a zgpr pulse sequence (with water suppression). Spectra were performed at 298 K with no purification step for all mutants. The spectrum was performed at 343 K for the ASRΔ2 alternan polymer after purification with dialysis using 14 kDa cutoff cellulose dialysis tubing (Sigma-Aldrich) in water.

For the wild-type enzyme and all variants (truncated forms and single and double mutants), differential scanning fluorimetry was performed with 7 μM pure enzyme in 50 mM sodium acetate buffer pH 5.75 supplemented with 0.5 $g \cdot L^{-1}$ of calcium chloride and 10× of SYPRO orange (Life Technologies). A ramp from 20 to 80 °C was applied with 0.3 °C increments on a C100 Thermal Cycler.

Crystallization and Data Collection. The initial conditions were screened using JCSG+ and PACT screens (QIAGEN). A Mosquito robot was used to make sitting drops by mixing 0.2 μL of enzyme solution with 0.2 μL of reservoir solution. The initial hits were reproduced, and diffraction-quality crystals of ASRΔ2 appeared after 3 months at 12 °C using 17% (w/v) PEG 3350, $NaNO_3$ 0.5 M as a precipitant, and an enzyme concentration of 8 $mg \cdot mL^{-1}$ with the presence of 10 mM isomaltohexaose (IM6). The crystal was cryoprotected in the reservoir solution supplemented with 15% (v/v) ethylene glycol and cryocooled directly in liquid nitrogen. Diffraction data were collected on beamline ID30A-3 of the European Synchrotron Radiation Facility (Grenoble, France).

Structure Solution and Refinement. Images were integrated using XDS[41] and converted to structure factors using CCP4 programs.[42] The structure was solved by molecular replacement using PHASER and the N-terminally truncated DSR-M as a search model (5LFC). To complete the model, cycles of manual rebuilding using COOT were alternated with automatic rebuilding cycles using BUCCANEER and refined using REFMAC5.[43] The final model was evaluated using the WHATIF[44] and MOLPROBITY[45] web servers and deposited in the PDB under the accession code 6HVG. To analyze the network of interactions in the structure, the RING[46] web server was used. Data collection and refinement statistics are shown in Table S2.

Structure Analysis, Manual, and Automated Docking. The ASRΔ2 and DSR-M (5NGY) domain V structures were aligned to manually dock the isomaltotetraose into the putative sugar binding pocket V-A of ASRΔ2. The ASRΔ2 and GTF180 (3HZ3 or 3KLL) structures were aligned to manually dock the sucrose or the maltose into the active site of ASRΔ2.

DOI: 10.1021/acscatal.8b04510
ACS Catal. 2019, 9, 2222−2237

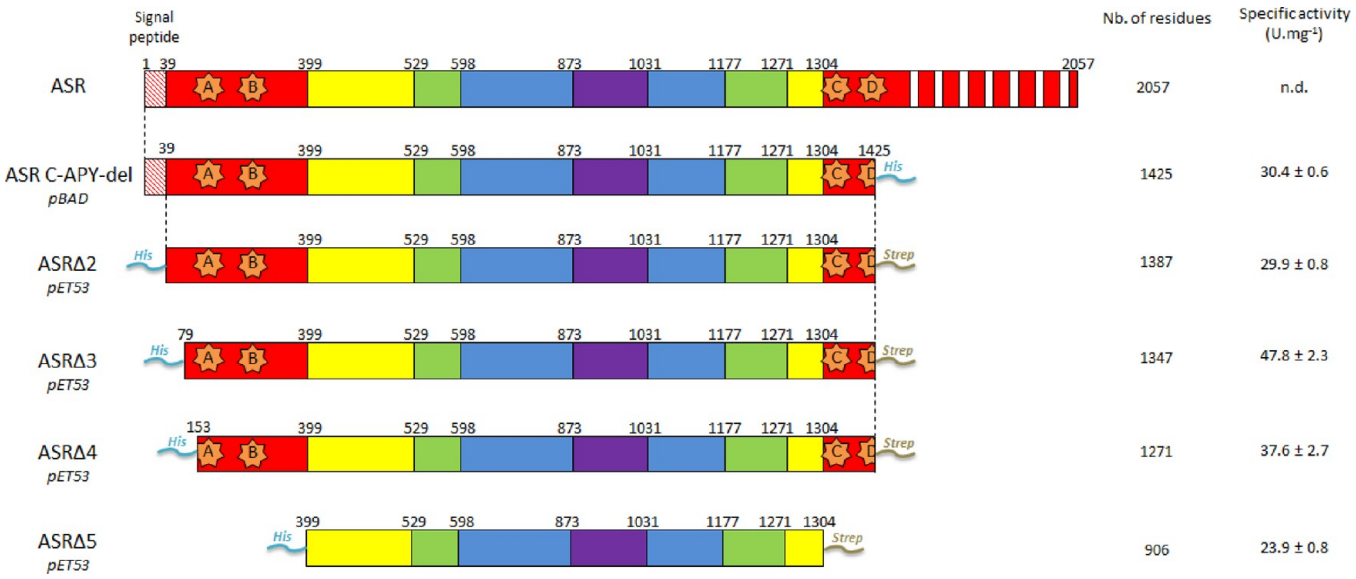

Figure 1. Schematic representation of the domain organization of ASR truncated mutants. Upper numbering corresponds to residues delimiting the different domains (red, domain V; yellow, domain IV; green, domain B;, blue, domain A; purple, domain C) predicted by alignment with DSR-M.[48] White stripes represent APY repeats.[11] Stars A (147−221), B (234−304), C (1324−1398), and D (1399−1425) represent the putative glucan binding pockets. His, His-tag; Strep, Strep-tag. Specific activities were determined from 292 mM sucrose in 50 mM sodium acetate buffer pH 5.75 at 30 °C and with 0.05 mg·mL^{-1} of pure enzyme.

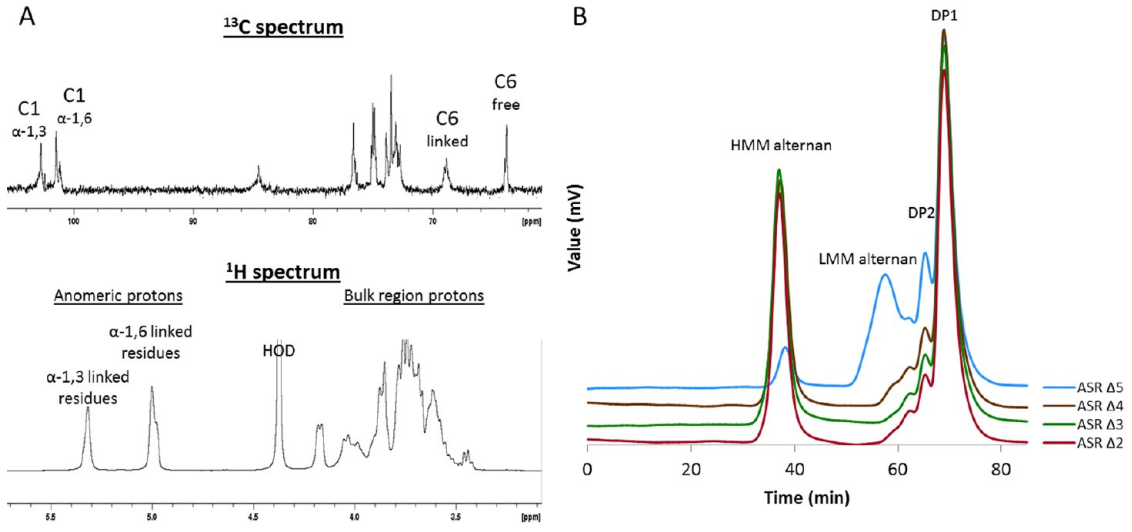

Figure 2. (A) ^{13}C and ^{1}H NMR spectra of alternan produced by ASRΔ2. ^{13}C spectrum: resonances at ∼102 and ∼101 ppm are attributed to the anomeric carbons involved in α-1,3 or α-1,6 linkages, respectively. At ∼84.5 ppm, the signal is assigned to C-3 of a C3-substituted glucosyl unit. Resonance of the various C-2, C-3, C-4, and C-5 of the glucosyl units arises between 75 and 70 ppm. At ∼68 and ∼63 ppm, signals correspond to the C-6 of the C-6-substituted glucosyl and to a free C-6, respectively. ^{1}H spectrum: signals at 5.32 and 5 ppm are assigned to the anomeric proton of glucosyl residues involved in α-(1→3), 39.5%, or α-(1→6)-linkage, 60.5%, respectively. This result is in accordance with the values reported in the literature for alternan.[8,11,15] (B) HPSEC chromatograms of truncated mutants. Reaction from sucrose at 30 °C with 1 U·mL^{-1} of pure enzyme and sodium acetate buffer 50 mM pH 5.75.

For the docking calculations, a model of the ASRΔ2 glucosyl−enzyme intermediate was constructed based on the high-resolution structure of the GH13 covalent intermediate (PDB 1S46). Oligosaccharide structures were built using the Glycam server (Woods Group. (2005−2018) GLYCAM Web. Complex Carbohydrate Research Center, University of Georgia, Athens, GA. (http://glycam.org)). Receptor and ligand structures were prepared with Autodock Tools and docked using Vina-Carb.[47] Representative structures were selected from all of the resulting conformers to meet a distance criterion of ≤3.5 Å from the O3 or O6 hydroxyl groups of the nonreducing terminal glucose to both the C1 atom of the glucosyl−enzyme intermediate and the side chain of the acid/base catalyst (E673).

RESULTS

Design and Characterization of Truncated Mutants.

As revealed by sequence alignment, ASR from *L. citreum* NRRL B-1355 is predicted to adopt the same fold as the other GSs comprising five domains A, B, C, IV, and V (Figure 1). To overcome the difficulties of recombinant ASR (Met1-Ala2057) and ASR-C-APY-del (Met1-Gly1425) crystallization, we

DOI: 10.1021/acscatal.8b04510
ACS Catal. 2019, 9, 2222−2237

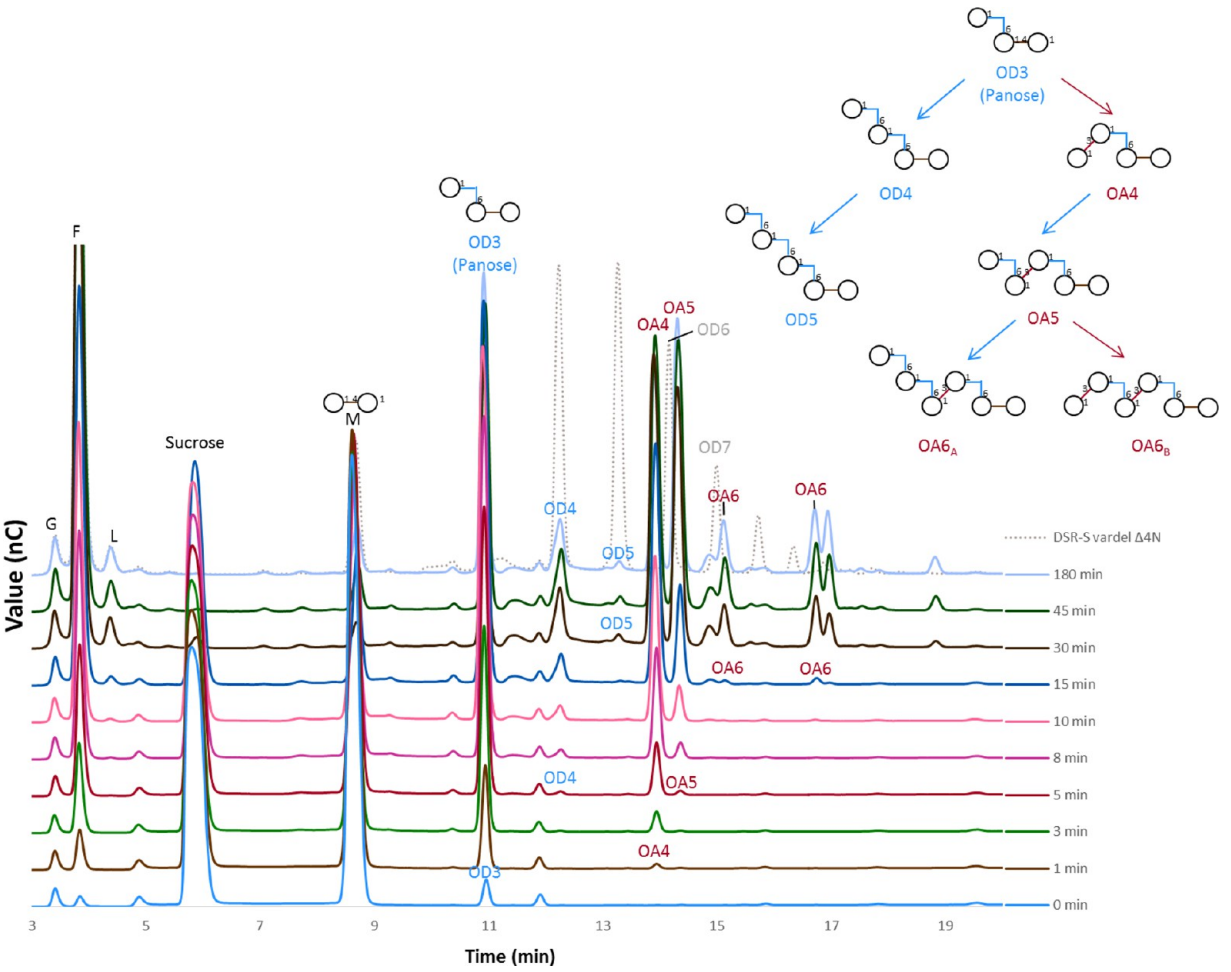

Figure 3. HPAEC monitoring of acceptor reaction of ASRΔ2 on maltose and model of product formation from maltose for DP 3 to 6. Adapted with permission from ref 40. Copyright 2006 Elsevier. Reaction from 292 mM of sucrose and 146 mM of maltose with 50 mM sodium acetate buffer pH 5.75 and 1 U·mL^{-1} of pure enzyme. G, glucose; F, fructose; L, leucrose; M, maltose; OD, oligodextran; OA, oligo-alternan.

constructed, produced, and purified several truncated forms: ASRΔ2, ASRΔ3, ASRΔ4, and ASRΔ5, deleted, respectively, of the signal peptide (Met1-His38), one predicted disordered region (Met1-Asp78), two predicted disordered regions (Met1-Pro152), and the entire domain V (Met1-Ser398 and Gln1305-Gly1425) (Figure 1).

The deletions did not severely compromise the specific activity of the truncated proteins. ^{1}H NMR and ^{13}C NMR analysis of the purified polymer synthesized by ASRΔ2 revealed the presence of 39.5% α-1,3 and 60.5% α-1,6 linkages (Figure 2A). ^{1}H NMR of the nonpurified glucans produced by the others variants were all similar (Figure S2). HPSEC analyses further showed that similar amounts of LMM and HMM polymers were produced with all of the truncated mutants except ASRΔ5 (Figure 2B). Indeed, the deletion of domain V strongly affects the ability to synthesize HMM alternan, as only 4.5 ± 0.2% of the glucosyl units from sucrose are incorporated into HMM polymer compared with 32.4 ± 0.8% in the case of ASRΔ2. The denaturation patterns of the variants, monitored using differential scanning fluorimetry (DSF), revealed two distinct transition temperatures for all of the variants, one around 37 °C and the other one around 55.0 °C. Such profiles are often encountered for multidomain enzymes. The melting temperatures (T_m) of ASRΔ2, ASRΔ3, and ASRΔ4 are in the same range. The two melting temperatures of ASRΔ5 are slightly lower, suggesting that domain V of ASR might contribute to overall enzyme stability (Figure S3).

Oligosaccharide Synthesis from Maltose Acceptor Reaction. An acceptor reaction with maltose, the best known acceptor for ASR, was carried out to ensure that the truncated mutants behaved in the same way as the full-length enzyme. First, acceptor reaction product formation was monitored using ASRΔ2 (Figure 3). Our results are in alignment with those of Côté et al. obtained using the native ASR.[49] To summarize, maltose undergoes α-1,6 glucosylation alone to give the oligodextran of DP3 (OD3 panose, α-D-Glc*p*-(1→6)-α-D-Glc*p*-(1→4)-D-Glc), which can be further elongated at either the O6 or the O3 position of the nonreducing unit to give the structures OD4 (α-D-Glc*p*-(1→6)-α-D-Glc*p*-(1→6)-α-D-Glc*p*-(1→4)-D-Glc) and OA4 (α-D-Glc*p*-(1→3)-α-D-Glc*p*-(1→6)-α-D-Glc*p*-(1→4)-D-Glc), respectively. The oligosaccharide OA4 was quick to appear at the beginning of the reaction (1 min) and accumulated at a much higher level than OD4, indicating that panose is preferentially elongated with an α-1,3 linkage. Note that a very small peak of OD5 originating from OD4 only appeared toward the end of the reaction (~30 min) and was not elongated further (no OD6 was found). As soon as the OA4 starts to accumulate, it is efficiently converted to OA5 (α-D-Glc*p*-(1→6)-α-D-Glc*p*-(1→3)-α-D-Glc*p*-(1→6)-

DOI: 10.1021/acscatal.8b04510
ACS Catal. 2019, 9, 2222−2237

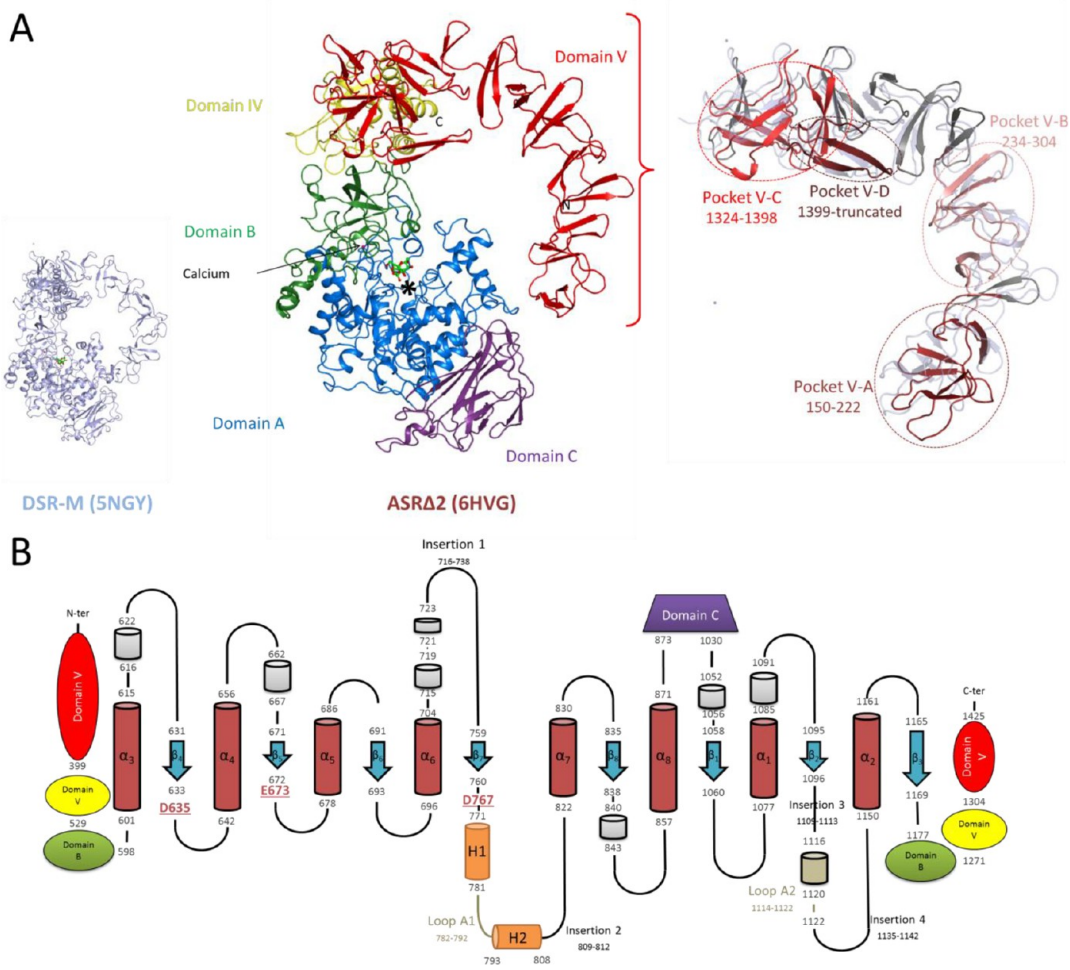

Figure 4. (A) Global view of the domain organization of ASRΔ2 (PDB ID 6HVG, chain A) versus DSR-M (PDB ID 5NGY, chain A) and zoom on ASRΔ2 domain V with the putative sugar binding pockets (circled). Star, active site. Red, domain V (147−398 + 1304−1424); yellow, domain IV (399−528 + 1271−1303); green, domain B (529−597 + 1177−1270); blue, domain A (1031−1176 + 598−872); purple, domain C (873−1030). Sucrose (green) was manually docked from 3HZ3 complex.(B) Schematic representation of the structural elements of the catalytic barrel of ASR Cylinder, α-helix; arrow, β-sheet. Pink and cyan elements belong to the catalytic barrel. Orange, helices H1/H2. Residue underlined, catalytic residues.

α-D-Glc*p*-(1→4)-D-Glc). The OA5 itself can act as an acceptor for the formation of two OA6s (α-D-Glc*p*-(1→6)-α-D-Glc*p*-(1→6)-α-D-Glc*p*-(1→3)-α-D-Glc*p*-(1→6)-α-D-Glc*p*-(1→4)-D-Glc and α-D-Glc*p*-(1→3)-α-D-Glc*p*-(1→6)-α-D-Glc*p*-(1→3)-α-D-Glc*p*-(1→6)-α-D-Glc*p*-(1→4)-D-Glc). Other products eluted at retention times close to those of OA6 were identified. They probably correspond to minor products of DP greater than DP6 and could not be determined using our LC/MS apparatus (Figure S4). All of the truncated mutants behaved exactly like ASRΔ2 (Figure S5).

Overall 3D Structure of ASRΔ2. After extensive crystallization trials, the 3D structure of the unliganded ASRΔ2 was solved by molecular replacement using the structure of DSR-M as a template[48] and refined at 2.8 Å resolution. We did not manage to reconstruct the entire N-terminal part of the enzyme due to the poor quality of the density map in this region. We subjected the crystals to Edman sequencing, which revealed protein degradation during the crystallization process. The crystallized fragment started at Thr145 instead of Ala38, thus being an intermediate between the ASRΔ3 and the ASRΔ4 constructions. The final model corresponds to the largest structure solved so far in the GH70 family and includes residues Ser147−Ser1423 for chain A and residues Gln248−Ser1423 for chain B, for which the electron density was less well resolved in the N-terminal region.

Like all of the other glucansucrases of solved 3D structure, ASRΔ2 comprises five distinct domains (A, B, C, IV, and V) in which domains A, B, IV, and V are made up by sequence fragments on either side of domain C (Figures 1 and 4A). This domain (Ser873-Gln1030) is composed of 10 β-sheets forming a Greek key motif.[50] Compared to the other glucansucrase structures, it also contains two insertions (^{882}SSGKDLKDGE^{890} and ^{913}QDNS^{916}) and one additional β-hairpin (Thr991 to Glu1005) (Figure S6). Overall, the β-strands are longer and ASR domain C displays a higher number of ionic, $\pi-\pi$ stacking interactions and hydrophobic residues (Val, Leu, Ile, Phe) than its counterparts in the other GS structures (DSR-M, GTF-SI, GTF180, GTFA, and GBD-CD2).

ASRΔ2 adopts an overall "horseshoe shape" in which domain V (Ser147-Ser398 and Ala1304-Arg1424) is bending toward the catalytic domain as previously observed in DSR-M glucansucrase[48] (Figure 4A). This is not surprising as the two enzymes share 48% and 87% of their identity between the N-

DOI: 10.1021/acscatal.8b04510
ACS Catal. 2019, 9, 2222−2237

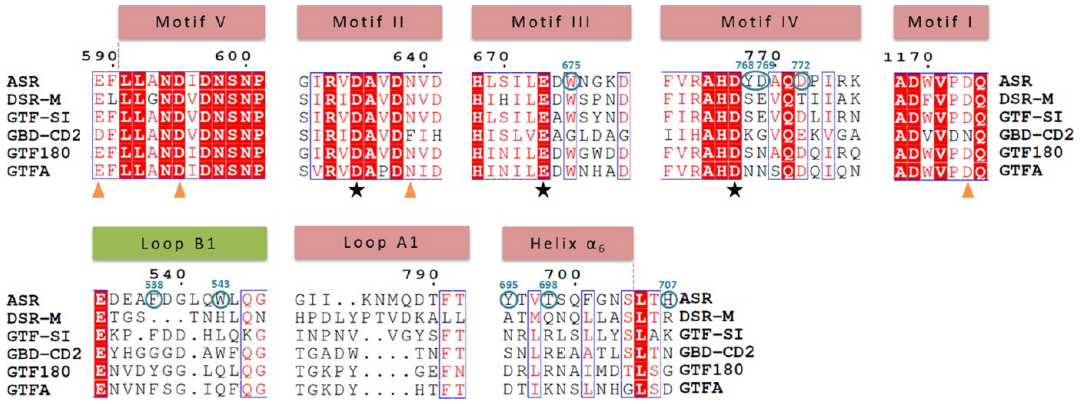

Figure 5. Partial alignment of sequences from available sucrose-active GH70 structures. Black star, catalytic residues. Orange triangle, calcium binding site (Glu589, Asp595, Asn639, and Asp1173). Cyan circled residues, residues targeted in this study. GenBank accession numbers, CAB65910.2 (ASR), CDX66895.1 (DSR-M), AAN58706.1 (GTF-SI), CDX66820.1 (GBD-CD2), AAU08001.1 (GTF180), AAU08015.1 (GTFA). Alignment created with ENDscript 2.[56] Structure-based sequence alignment is provided in Figure S9.

terminal and the C-terminal ends, respectively, of their domain V. This typical fold is due to the position of domain V relative to domain IV (Gln399-Asn528 and Gly1271-Asp1303) which is thought to act as a hinge between domain V and domains A/B, as previously proposed for the glucansucrases GTF180 and DSR-M.[48,51] Notably, the ASRΔ2 domain V shows repeated units composed of three consecutive β-hairpins with a hydrophobic core and many $\pi-\pi$ stacking interactions reinforcing their packing (Figure S7).[52,53] These super-secondary elements allow one to define four putative sugar binding pockets (named V-A, V-B, V-C, and V-D) in the global ASR sequence by sequence alignments and homology to the sugar binding pockets identified in DSR-E and DSR-M[48,52] (Figure 4A).

ASRΔ2 Catalytic Domain. The catalytic domain A of ASRΔ2 is formed by a $(\beta/\alpha)_8$ barrel common to all enzymes of the GH-H clan, which also comprises the GH13 and GH77 families. Compared with the $(\beta/\alpha)_8$ barrel of the GH13 family, the barrel of ASRΔ2 and of all other glucansucrases underwent a circular permutation occurring between strand β3 and helix α3 (Figure 4B). Consequently, the conserved and signature motifs I–IV are not placed in the same order along the sequence in the GH70 glucansucrases compared to those of GH13 family enzymes, motif I being downstream of motif II to IV in the sequences in the GH70 glucansucrases (Figure 5).[54] A manual docking of sucrose in ASRΔ2 was performed using the GTF180:sucrose complex (PDB ID 3HZ3). The residues defining subsites −1 and +1 of ASRΔ2 and GTF180 (according to the subsite nomenclature proposed by Davies et al.[55]) and in interactions with the glucosyl and the fructosyl ring of sucrose, respectively, were similar. They were well aligned with a RMSD of 0.33 Å and confirmed that the catalytic residues of ASRΔ2 are Asp635, Glu673, and Asp767 (Figure S8).[53] Compared to DSR-M and GTF180, domain A of ASRΔ2 (Asn598-Val872 and Asp1031-Tyr1176) displays several insertions in the loops emerging between (i) α-helix 6 and β-strand 7 (insertion 1, Trp716-Arg738), (ii) β-strand 7 and α-helix 7 (insertion 2, ^{809}NPSG^{812}), and (iii) β-strand 2 and α-helix 2 (insertion 3, ^{1109}NYGGM^{1113}; insertion 4, ^{1135}NKADGNPN^{1142}) (Figures 4B and 6A).

A calcium ion is present at the interface between domain A and B in interaction with Glu589, Asp595 (motif V), Asp1173 (motif I), and Asn639 (motif II) (Figure 5), similar to the situation already described for GTF180.[53] The effect of calcium on ASRΔ2 was investigated by comparing the specific activities obtained without calcium ion addition and in the presence of 3.4 mM calcium chloride or with 5 mM EDTA. The values were 29.9 ± 1.0, 33.6 ± 2.6, and 29.5 ± 1.0 U·mg^{-1}, respectively, indicating that calcium ions do not significantly activate the enzyme as previously reported for the ASR of *L. citreum* ABK-1, for which a 1.2-fold increase in activity was observed in the presence of 10 mM calcium chloride at 40 °C pH 5.[23] However, the absence of calcium influenced the enzyme denaturation profile during DSF experiments and led to an almost complete elimination of the higher transition at 55 °C (Figure S3).

All of the secondary structural elements of the barrel superpose well with those of the other GH70 structures solved so far, except the α-helix H1 (Gln771-His781) and α-helix H2 (Phe793-Glu808) between β-strand 7 and α-helix 7, for which we observed the largest deviation. This could be due to rearrangements triggered by the presence or absence of ligand in the active site, as shown for DSR-M,[48] and/or to the flexibility of this region. Indeed, the H1/H2 (Gln771-Glu808) helices present a relatively high B-factor with an average of 66.4 Å^2 compared to 56.4 Å^2 for domain A.

Focusing on the Catalytic Core To Investigate Linkage Specificity and HMM Polymer formation. Two different zones surrounding the sucrose molecule in the model of ASRΔ2:Sucrose complex drew our attention (Figure 6B). The first, zone 1, comprises **Trp675**, **Tyr695**, **Thr698**, **His707**, **Tyr768**, and **Asp769.** Trp675 is a conserved residue (in motif III), located between subsites +1 and +2 (Figure 6B, Figure S8). The other four residues are in the proximity of Trp675. In particular, Tyr768 and Asp769 form part of the triplet ^{768}YDA^{770} (in motif IV following the TSS), which is unique to alternansucrases and is replaced by the triplet SEV in most dextransucrases (DSR-S) and mutansucrases (GTF-I) or by the triplet NNS in reuteransucrases (GTFA). The second region of interest, zone 2, is located on the opposite side of zone 1 (Figure 6B) and comprises residues that could define a path to the sucrose binding site including **Trp543, Asp772**, and **Phe538.** The Trp543 residue is unique to ASRΔ2 and located in a small α-helix (Leu541-Gln545) of loop B1 (Glu534-Gly548). Behind this residue, Phe538 is not strictly conserved in glucansucrases. Finally, Asp772 in α-helix H1 is facing Trp543 and points toward the active site. A total of nine positions were selected and mutated to examine their role in

DOI: 10.1021/acscatal.8b04510
ACS Catal. 2019, 9, 2222–2237

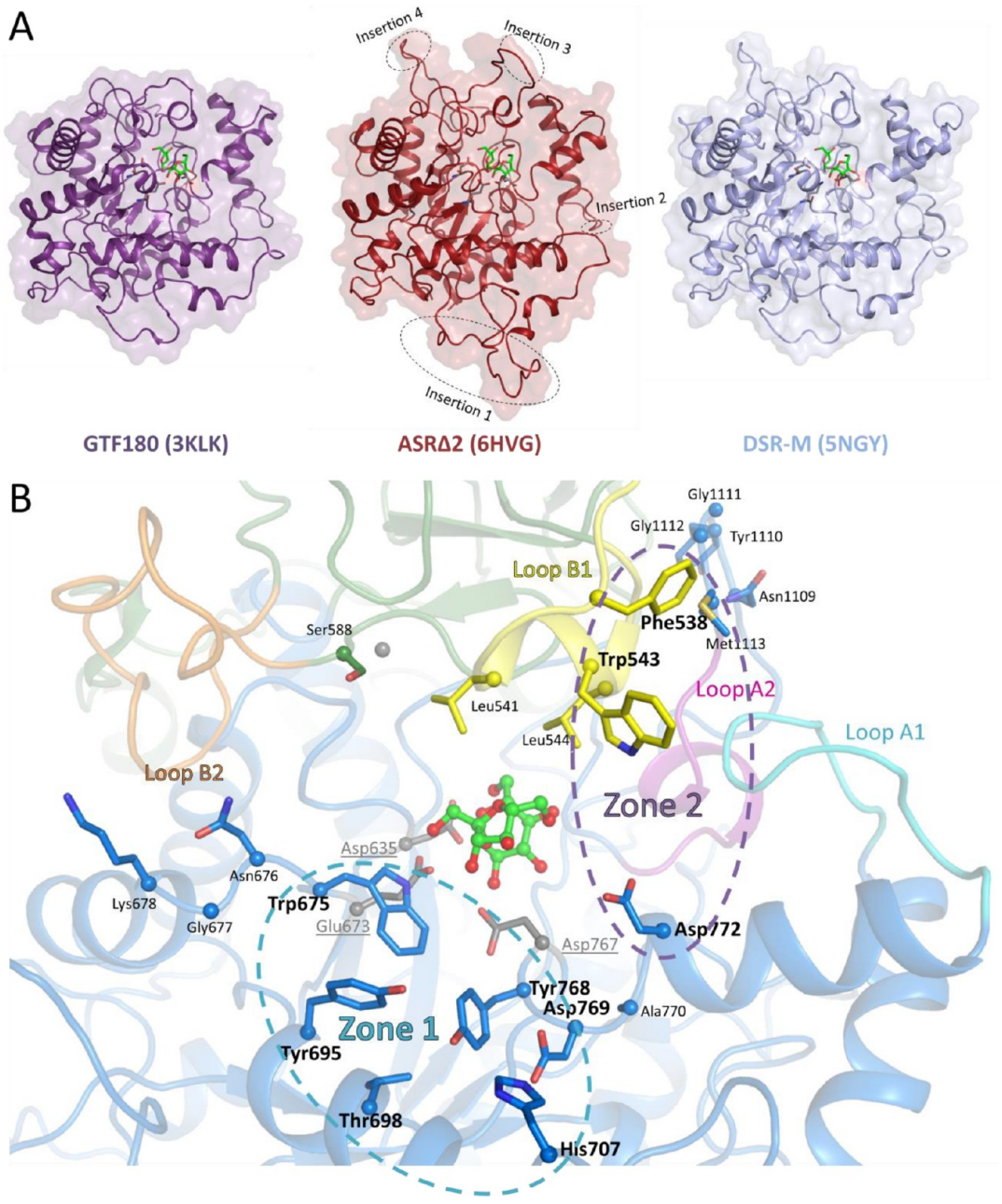

Figure 6. (A) View of the insertions in domain A of ASRΔ2 compared to GTF180 and DSR-M. Only domain A is shown. Insertion 1: 716−738. Insertion 2: 809−812. Insertion 3: 1109−1113. Insertion 4: 1135−1142. (B) View of the catalytic site and loop positioning in ASRΔ2. Residues targeted are in bold. Catalytic residues are underlined in gray. Loop A1: 782−792. Loop A2: 1114−1122. Loop B1: 534−546. Loop B2: 570−587. Navy blue: domain A. Forest: domain B. Gray sphere: calcium. Green: sucrose (docked from 3HZ3).

specific activity, linkage specificity, stability, or ability to synthesize HMM polymer (Figure 6B). The results are shown in Table 1.

Mutations in Zone 1: Impact on Specificity and HMM Polymer Synthesis. Trp675 was swapped with Ala, Phe, Tyr, or His residues. All of the mutants were impacted in their specific activity, in particular, the Ala and His mutants (10% and 2.6% residual activity). Except for Trp675Phe, all of them produced much lower amounts of HMM polymer and higher amounts of glucose, showing that the mutation favored the hydrolysis reaction (Figure 7A). Mutation Trp675Phe was highly detrimental to the enzyme's stability, as reflected by a ΔT_m of −17 °C compared to the wild type. Overall, the linkage specificity was not affected by the mutations at this position, suggesting that this zone does not contribute to α-1,3 glucosylation. Indeed, the Trp675Ala mutation did not disfavor the formation of OA4 (Figure S10).

Mutants Tyr695Ala, Thr698Ala, and His707Ala synthesized equivalent amounts of HMM polymer and α-1,3 linkages to the wild type. Individually, these positions do not seem to be highly critical for polymer elongation and linkage specificity. Considering the tyrosine 768 of YDA motif though, our results indicate that it is different. Replacing Tyr768 with a Phe results in an enzyme that acts similarly to the parental enzyme, with the main function of the Tyr residue probably being maintained. In contrast, the Tyr768Ala mutant as well as the Tyr695Ala-Tyr768Ala double mutant induce a slight increase in α-1,6 linkage synthesis (+6% and 8%, respectively),

DOI: 10.1021/acscatal.8b04510
ACS Catal. 2019, 9, 2222−2237

Table 1. Biochemical Data on Mutants from the Catalytic Site[a]

	localization	residual specific activity (%)	ΔT_m with the wild-type enzyme (°C)	α-1,3 linkages (%, NMR)[b]	α-1,6 linkages (%, NMR)[b]	HMM polymer (%, HPSEC area)	hydrolysis (%)
wild type							
ASRΔ2 WT		100 ± 3.3	0	35	65	32.4 ± 0.8	4.4 ± 0.5
zone 1							
ASRΔ2 W675A	motif III second residue downstream of the acid/base	10.0 ± 0.77	−3.3	31	69	5.7 ± 0.3	44.9
ASRΔ2 W675F		32.4 ± 0.54	−16.8	39	61	31.0 ± 0.2	4.8
ASRΔ2 W675Y		35.1 ± 1.2	−1.8	28	72	8.6 ± 0.2	6.1
ASRΔ2 W675H		2.6 ± 0.06	−2.6	39	61	11.3 ± 0.2	12.3
ASRΔ2 H707[c]A	helix α_6	120.4 ± 9.0	−0.1	35	65	34.1 ± 0.3	4.3
ASRΔ2 T698[c]A		85.3 ± 0.67	−2.1	36	64	34.5 ± 0.2	4.4
ASRΔ2 Y695[c]A		61.9 ± 2.5	0.8	33	67	27.3 ± 0.1	5.2
ASRΔ2 Y768[c]A	motif IV "YDA" sequence downstream of the TSS	54.2 ± 2.9	−1.9	29	71	21.0 ± 0.1	6.5
ASRΔ2 Y768[c]F		110.4 ± 2.5	0.4	35	65	33.6 ± 0.2	6.1
ASRΔ2 Y768[c]W		52.8 ± 1.6	−0.8	29	71	11.9 ± 0.2	5.2
ASRΔ2 D769[c]A		110.4 ± 2.0	−0.8	29	71	26.0 ± 0.2	5.8
ASRΔ2 Y695[c]A + Y768[c]A		67.2 ± 3.0	−0.3	27	73	18.3 ± 0.04	6.1
zone 2							
ASRΔ2 F538A	loop B1	95.3 ± 5.4	−4.7	37	63	31.9 ± 0.2	4.5
ASRΔ2 W543[c]A		78.5 ± 7.7	1.3	24	76	14.8 ± 0.1	7.2
ASRΔ2 D772A	helix H1	36.5 ± 2.5	0.4	5	95	3.2 ± 0.1	5.1
ASRΔ2 D772E		71.9 ± 5.7	−1.8	7	93	10.9 ± 0.1	5.4
ASRΔ2 D772Y		36.1 ± 1.7	0	6	94	3.9 ± 0.1	5.1
ASRΔ2 W543[c]A + D772A		63.9 ± 2.6	0	6	94	2.1 ± 0.04	5.4

[a]Reaction from sucrose only at 30°C with 1 U·mL^{-1} of pure enzyme and sodium acetate buffer 50 mM pH 5.75. [b]NMR was performed on crude reaction medium. [c]Residues specific to alternansucrases. Specific activity of ASRΔ2: 29.9 ± 1.0 U·mg^{-1}. Four different wildtypes ASRΔ2 were characterized. Specific activity was determined in triplicate for the same sample. T_m was determined by DSF.

suggesting that this zone might have a subtle but specific role in the formation of the α-1,6 linkages, also observed in the increased formation of OD oligosaccharides (oligodextran series) compared with the wild-type enzyme (Figure 8). HMM polymer formation decreases from 33% for the wild type to 20% and 12% for the Tyr768Ala and Tyr768Trp mutants, respectively.

Mutations in Zone 2: Impact on Specificity and HMM Polymer Synthesis. The most spectacular effect concerns the mutations introduced at position 772 of helix H1 and to a lesser extent at position 543 of loop B1 (Figure 7B). The specific activity values of mutants Asp772 Ala/Glu/Tyr decreased, representing 36.5%, 71.9%, and 36.1% of that of the wild-type enzyme, respectively. They all produced much lower quantities of HMM polymer, although the hydrolysis activity is almost unchanged compared to wild-type ASRΔ2. The synthesis of α-1,6-linked oligomers is clearly favored, and the ability to synthesize α-1,3 linkages is almost lost (5%). In comparison, mutant Trp543Ala followed the same trend, even if the reduction of α-1,3 linkage synthesis and the impact on HMM polymer formation is less dramatic. The Trp543Ala-Asp772Ala double mutant behaves like the Asp772 single mutant, suggesting that the most important residue for α-1,3 glucosylation is Asp772. Finally, mutant Phe538Ala acts similarly to the wild type. The HPAEC chromatograms of the products of the maltose acceptor reaction also shed similar light. All of the Asp772 mutants produce more OD oligosaccharides than the wild type. To illustrate, in Figure 8 we provide the most striking chromatographic profiles of the Tyr768Ala mutant and the Asp772Ala-Trp543Ala double mutant. Remarkably, it can be seen that the double mutant is even able to produce a small amount of OD6.

DISCUSSION

Alternansucrase from *L. citreum* B-1355 has always been regarded as an intriguing glucansucrase, first because of its unusual ability to synthesize alternating α-1,3 and α-1,6 in the polymer chain and also because of its thermal stability. By solving the structure of this enzyme, we intended to bring new insights into the structural determinants influencing those highly unusual traits.

Contribution of Different Structural Features Influencing ASR Stability. The X-ray structure of ASRΔ2 is typical of GH70 glucansucrases. Its closest counterpart, in terms of sequence and 3D structure similarities, is DSR-M, which also exhibits a horseshoe shape with a domain V in close proximity to the catalytic domain A/B. The stability of the entire edifice is clearly enhanced by calcium coordination that likely reinforces the interaction between domains A and B. Domain V is another contributor to stability as ASRΔ5 is the least stable enzyme of the truncated forms generated in our study. Although it is counterintuitive, the insertions (1−4) increasing the length of several loops on the enzyme surface could also contribute to enzyme stability. Indeed, it is generally thought that long loops in proteins decrease stability by increasing local flexibility and propensity to aggregate.[57] In ASRΔ2, the shape of these loops may prevent solvent penetration. Insertion 3 belonging to domain A

DOI: 10.1021/acscatal.8b04510
ACS Catal. 2019, 9, 2222−2237

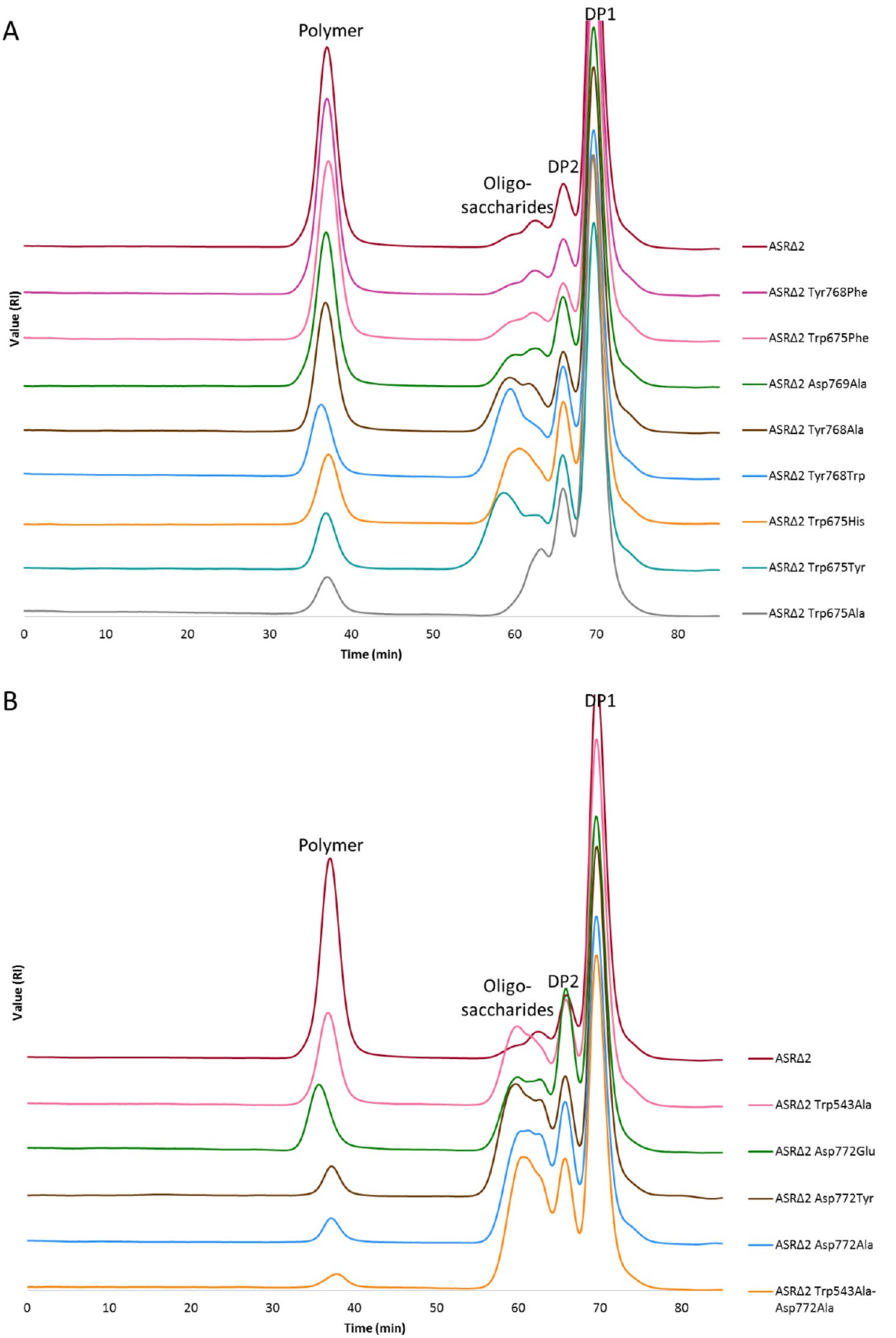

Figure 7. (A) HPSEC chromatogram of zone 1 mutants. Mutants with slight effect are not depicted (Tyr695Ala, Tyr695Ala-Tyr768Ala, His707Ala, Thr698Ala). (B) HPSEC chromatogram of zone 2 mutants.

(^{1109}NYGGM^{1113}) appears ideally located to protect some of the residues underneath that form the side wall of the catalytic pocket (Tyr1176, Leu592) (Figure 6B). Finally, the domain C of ASRΔ2 displays structural features (longer β-strands, higher

DOI: 10.1021/acscatal.8b04510
ACS Catal. 2019, 9, 2222−2237

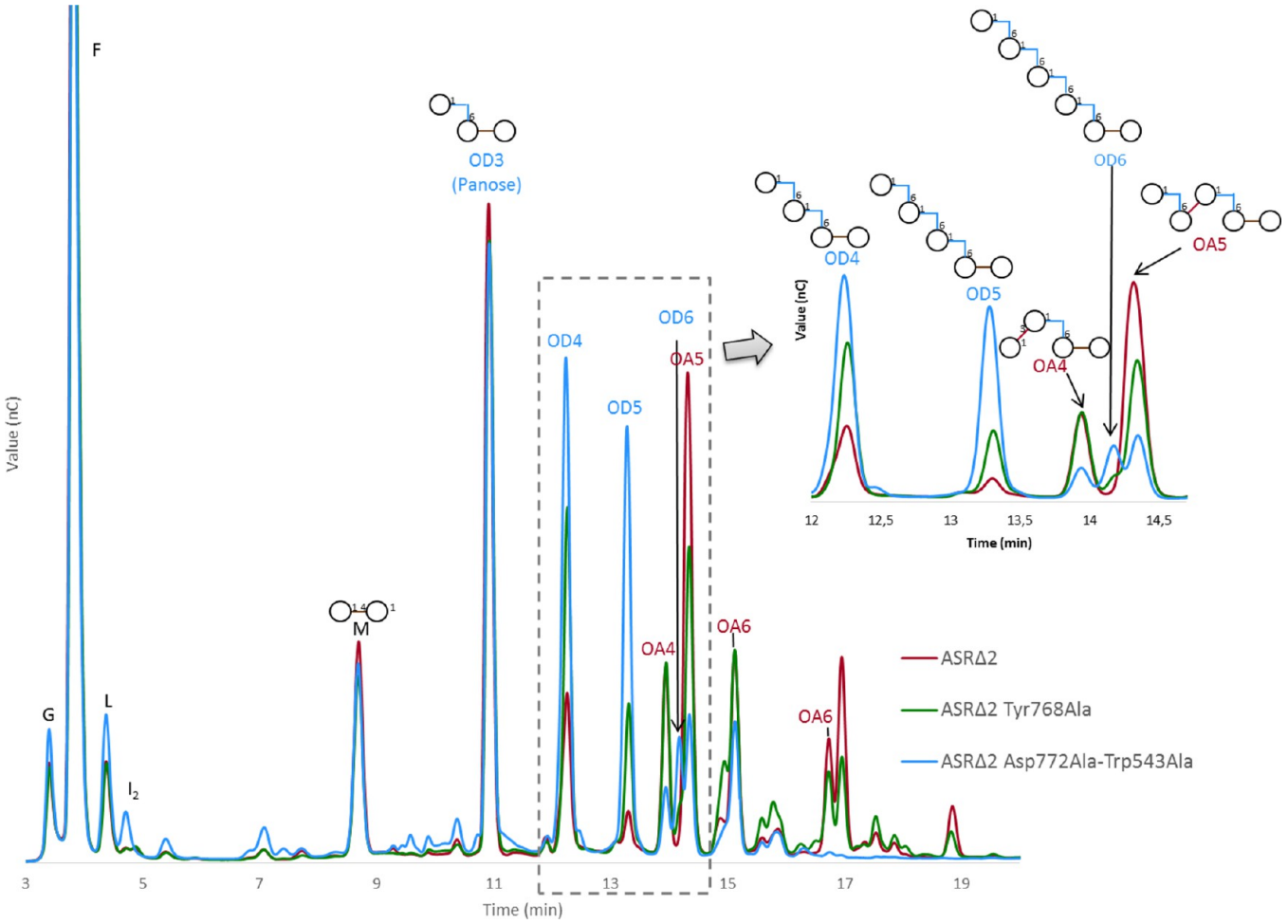

Figure 8. HPAEC chromatogram of ASRΔ2 compared to mutant Tyr768Ala and double-mutant Asp772Ala-Trp543Ala. Reaction from 292 mM sucrose and 146 mM maltose with 50 mM sodium acetate buffer pH 5.75 and 1 U·mL^{-1} of pure enzyme. G: Glucose. F: Fructose. L: Leucrose. M: Maltose. OD: Oligodextran. OA: Oligo-alternan of different DP.

number of hydrophobic residues, $\pi-\pi$ stacking, and ionic interactions) that could reinforce its role of "pedestal" at the bottom of the U-shaped fold and provide a contribution to enzyme stability. This warrants further investigation.

HMM Alternan Formation Is Controlled by Catalytic Core Residues and by Domain V. The Trp675 residue belonging to zone 1 is important for the formation of HMM alternan synthesis. It provides a critical stacking platform defining subsite +2 and accommodates sugar acceptors as previously suggested for Trp1065, the corresponding residue in GTF180. Indeed, 10 mutants of Trp1065 were shown, in GTF180, to totally lose their ability to synthesize HMM polymer. Only the mutant Trp1065Phe still produced HMM polymer but in very small amounts (just 2.2% compared with 16.5% for wild-type GTF180).[58] In ASRΔ2, the Trp675Phe mutation was much less detrimental to HMM polymer formation than in GTF180. Overall, and even though the number of α-1,3 linkages obtained with mutant Trp675Tyr decreases slightly, mutation of Trp675 does not greatly impact enzyme linkage specificity. However, the factor with greatest influence on HMM alternan formation seems to be the presence of domain V as the ASRΔ5 truncated form produces very small amounts of polymer. We can submit that the putative sugar binding pockets identified contribute to polymer elongation as proposed for DSR-M.[48] Future biochemical studies should confirm the functionalities of these pockets.

Understanding α-1,6 Linkage Specificity through the Recognition of Different DP2 Acceptors. To gain a better understanding of the efficiency of maltose, nigerose, and isomaltose as acceptors, here ranked in decreasing order of efficiency,[20,39] we docked each disaccharide in the ASR active site (Figure 9). The superposition of the GTF180-maltose complex on ASRΔ2 (Figure 9A) shows that the site formed by Asn639 and Trp675 is perfectly conserved and the maltose O6 hydroxyl (at the nonreducing end) is oriented toward the covalent intermediate, thus indicating that the mechanism already proposed for GTF180[53] to explain the α-1,6 specificity is very likely to operate for ASR. This is in alignment with previous observations[20,39] and with our own observations that, starting from maltose, only panose can be formed (Figure 8). Interestingly, our docking simulation found a binding pose for nigerose (Figure 9B) that closely mimics the GTF180 maltose complex, thus confirming that nigerose is also a good acceptor and can be efficiently elongated with an α-1,6 linkage from this subsite. In contrast, the docking failed to identify a similar binding pose for isomaltose (IM2) in this subsite. If we assume that the stacking interaction with Trp675 is a requisite for acceptor binding, the lack of a binding pose may be explained by the presence of the bulky Tyr768 next to the Trp675, which

DOI: 10.1021/acscatal.8b04510
ACS Catal. 2019, 9, 2222−2237

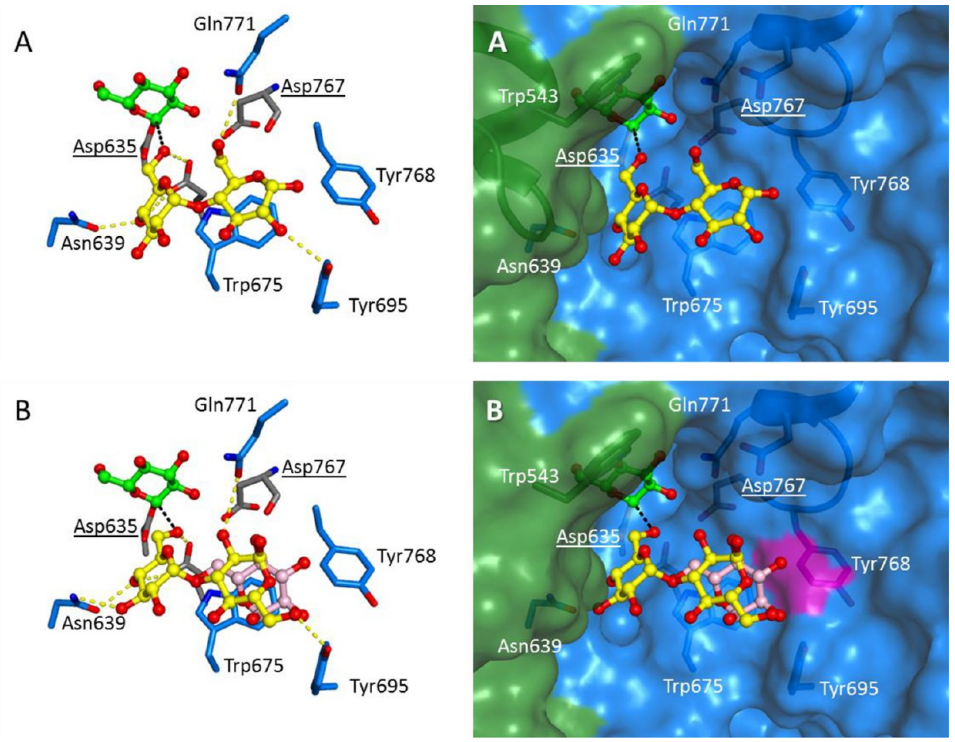

Figure 9. (A) Maltose from GTF180 (3kll) manually superposed on the catalytic cleft of the ASR. (B) Nigerose is docked automatically (yellow), and isomaltose is manually superposed (light pink) to illustrate the steric clash with Tyr768 (magenta). Two different representations are shown: catalytic triad is colored in gray, and covalent intermediate is colored green. Direction of attack of the acceptor is indicated by a dashed black line, and all possible polar contacts are shown by dashed yellow lines.

could lower the affinity of this site for IM2. This hypothesis is confirmed by the Tyr768Ala mutant, which indeed produces higher amounts of oligodextrans from the maltose acceptor reaction (Figure 8), suggesting that the Tyr768Ala mutation has opened the way for the accommodation and synthesis of α-1,6 isomaltooligosaccharides. Also, in accordance with this suggestion, the content of α-1,6 linkage in HMM glucan also increased by 6% for this mutant and by 8% for the Tyr768Ala-Tyr695Ala double mutant. All of our data are indeed in accordance with the previous finding that isomaltose is not as good an acceptor as nigerose and maltose.[20,39] Moreover, comparison of ASR with GTF180 and DSR-M (both being more specific for α-1,6 linkage synthesis) shows that Tyr768 is replaced by a serine. Furthermore, in both GTF180 and DSR-M a second Trp residue is present in close proximity to the first stacking tryptophan. Given the importance of carbohydrate−aromatic interactions, we could hypothesize that this additional Trp might form an extended binding platform, not therefore present in the ASR, for oligosaccharide binding in this area (Figure 10).

Control of α-1,3 Linkage Introduction Is Mediated by Another Subsite. If we assume that only α-1,6 glucosylation is possible from the first acceptor site (Asn639, Trp675), another mechanism should occur in a different location in the catalytic cleft that could explain the α-1,3 glucosylation. Indeed, the mutations operated in zone 2 and particularly on Asp772 and Trp543 led to a drastic decrease in α-1,3 linkage formation in both the HMM polymer obtained from sucrose and the oligosaccharides formed by the acceptor reaction with maltose. The phenomenon was more severe for mutation on Asp772. To investigate this possibility, we performed docking of α-D-Glc*p*-(1→6)-α-D-Glc*p*-(1→3)-D-Glc and isomaltotriose (IM3) into the catalytic cleft of ASR with the aim of identifying the best poses that oriented the O3 hydroxyl of the nonreducing glucosyl at a distance conducive to nucleophilic attack on the covalent intermediate. For IM3, the most representative acceptor pose is ensured as a result of interaction of the O6 of nonreducing terminal glucosyl with Asn639 and Glu673 (the acid/base), Asp767 (the transition state stabilizer), the middle glucosyl ring with Gln771, and Asp772 (defining +2′ subsite), further reinforced by a stacking interaction with Trp543 (defining +3′ subsite) (Figure 11A). On the basis of this mode of interaction we can submit that Trp543 has a role in capturing the acceptors, bringing them into the proximity of the active site (elongation mainly affected by mutation on Trp543), while the correct positioning of the acceptor is ensured by Asp772 and a network of interactions (Figure 11). A very similar positioning is obtained for α-D-Glc*p*-(1→6)-α-D-Glc*p*-(1→3)-D-Glc, showing that acceptors with alternated linkages are accommodated well in subsite +2′ (Figure 11B). It is noteworthy that our mutation Asp772Glu has the same global effect on linkage specificity as an Ala substitution (near-complete loss of α-1,3). Only an Asp side chain, which is shorter and less flexible than a Glu side chain, can control this very precise accommodation leading to α-1,3 glucosylation.

Interestingly, Asp772 is conserved in 18 out of 63 sequences of biochemically characterized GH70 enzymes and essentially in enzymes synthesizing polymers mainly composed of α-1,3 linkages in their linear chains of insoluble α-1,3-linked mutant type. In most of the other sequences, a Thr is found at this position. Replacement of this aspartate with a Thr in mutant Asp567Thr GtfB from *S. mutans* GS5 or Asp569Thr GTF-I from *S. downei* MFe28 resulted in an increase in soluble glucan

DOI: 10.1021/acscatal.8b04510
ACS Catal. 2019, 9, 2222−2237

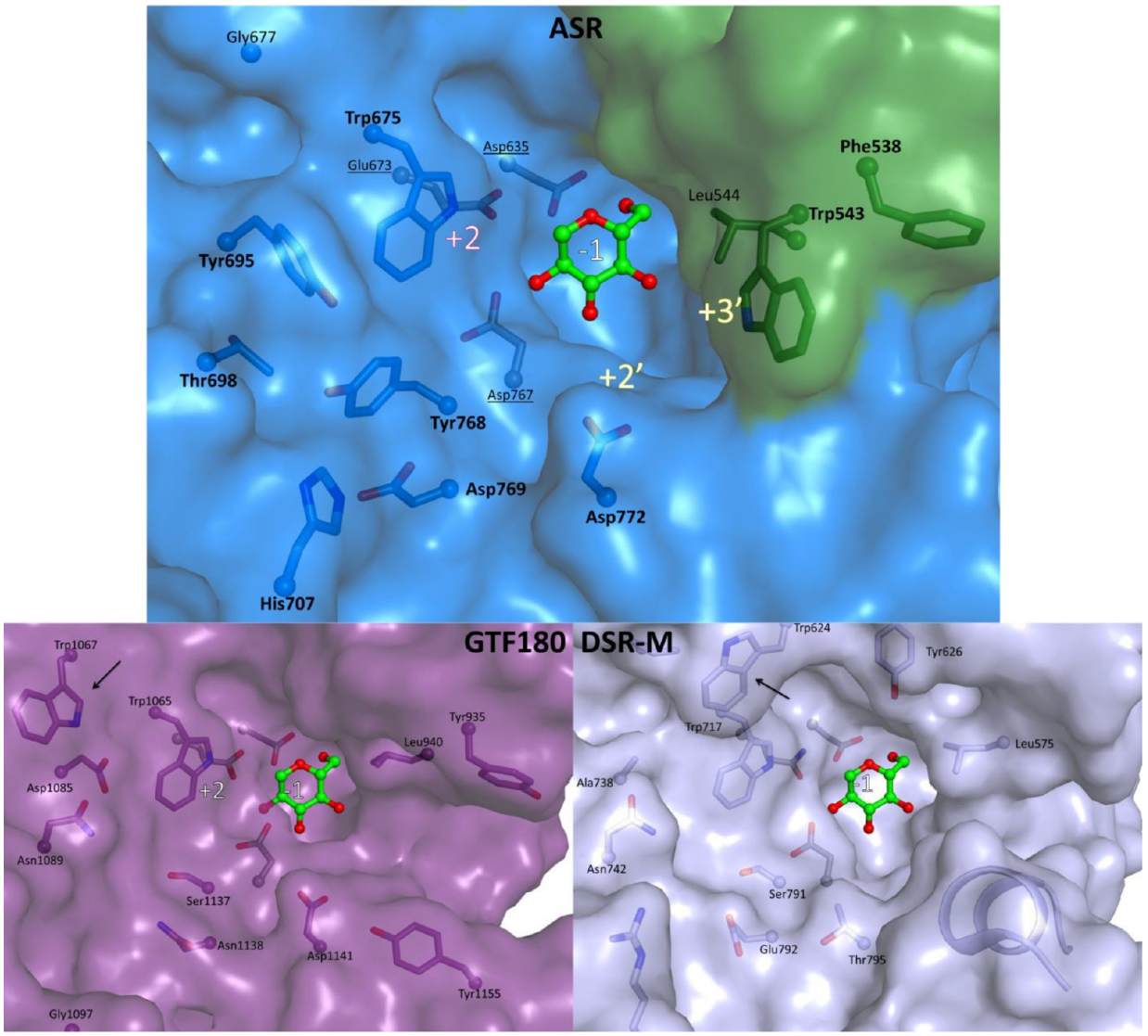

Figure 10. Comparison of the catalytic cleft and subsites of ASRΔ2, DSR-M, and GTF180. Residues targeted in this study in ASR are shown in bold.

formation presumably containing greater numbers of α-1,6 linkages.[59] Conversely, mutations Thr589Asp and Thr589Glu in GtfD from *S. mutans* GS5 (which synthesizes a soluble α-1,6-linked glucan) reduced soluble glucan production from 86% to 15% and 2%, respectively.[60] From our results, we can submit that the Asp residue in these proteins plays a similar role to that suggested in ASR. The role of Trp543 cannot be directly related to other studies as the residue is unique to ASR. However, our mode of acceptor binding in the +2′ subsite is close to what was already proposed by the docking calculation to explain the role of Leu940 in GTF180, the equivalent of Leu544 in ASR.[61] The Leu940Trp mutation completely abolishes α-1,3 glucosylation, showing that this region is clearly important for GTF180 linkage specificity. Additionally, dextransucrase DSR-M displays a threonine in place of the Asp772, and moreover, the presence of a short helix in this area prevents the existence of the equivalent of subsites +2′′ and +3′ for this enzyme (Figure 10). All of these observations suggest that the catalytic cleft of each GH70 enzyme has its own identity, expressed through an extremely precise interplay between the different residues and the loops surrounding the active site.

ASR Is Designed To Alternate α-1,6 and α-1,3 Linkages. Nigerotriose has never been described in alternan or in oligosaccharides formed from maltose[9,39] meaning that ASR is unable to α-1,3 elongate a terminal nigerose moiety. Docking of nigerose or α-D-Glc*p*-(1→3)-α-D-Glc*p*-(1→6)-α-D-Glc failed to identify acceptable binding poses in the +2′ subsite that could lead to α-1,3 glucosylation. The formation of two consecutive α-1,3 linkages may be disfavored for the following reasons: (i) the specific interaction with Asp772 will necessarily be disrupted by the presence of an O3 substituent and (ii) the shortness and rigidity of an α-1,3 linkage (compared to an α-1,6) will position the nonreducing glucosyl either too far from the covalent intermediate or in a poor orientation, which will result in a nonproductive complex. We cannot totally exclude the possibility (although to a limited extent) of consecutive α-1,6 linkage formation from the +2′ subsite due to the flexibility of the α-1,6 linkage. In addition, we do not explicitly address the question of branch formation. However, the active site is wide, and the presence of both

DOI: 10.1021/acscatal.8b04510
ACS Catal. 2019, 9, 2222−2237

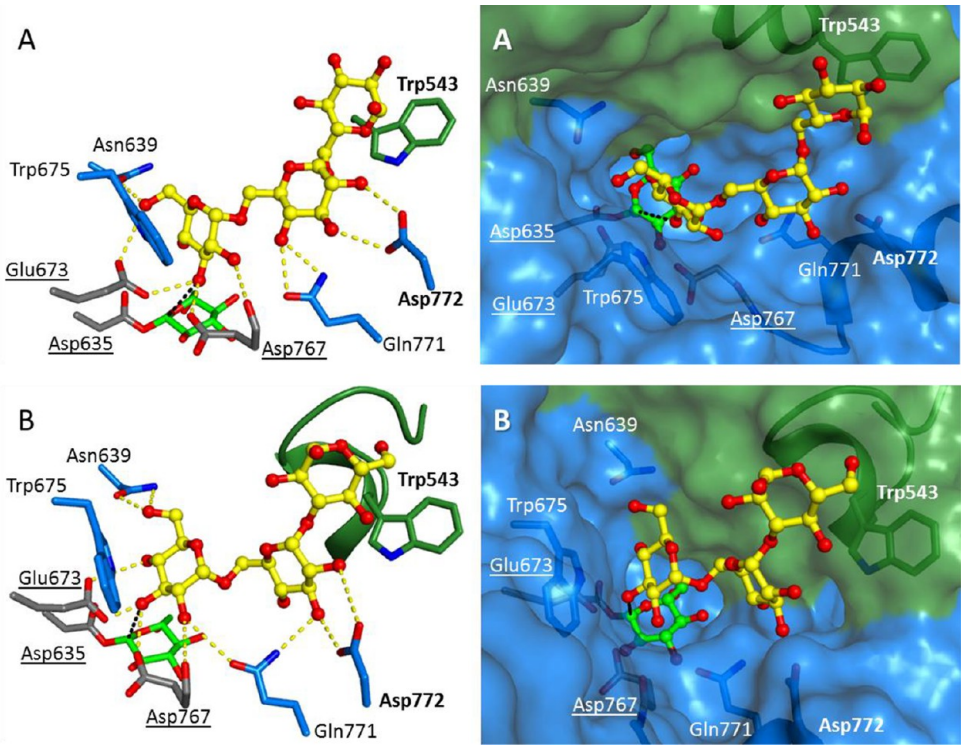

Figure 11. Isomaltotriose (IM3) (A) and α-D-Glc*p*-(1→6)-α-D-Glc*p*-(1→3)-D-Glc (B) are automatically docked to illustrate α-1,3 glucosylation. Two different representations are shown: catalytic triad is colored in gray, and covalent intermediate is colored in green. Direction of attack of the acceptor is indicated by a dashed black line, and all possible polar contacts are shown as dashed yellow lines.

subsites +2 and +2′ bordering subsite +1 should allow for alternative accommodations of isomaltotriosyl units and explain the presence of 3,6-disubstituted glucose in alternan (Figure S11).

Bringing together all our data, we submit that α-1,3 linkage formation is governed by the +2′ subsite with the help of Asp772, only if the acceptor is previously α-1,6 linked. The formation of consecutive α-1,3 linkages is prevented, and further elongation of an α-1,3-linked moiety will continue only with an α-1,6 linkage. Comparison of the binding modes leading to either α-1,6 or α-1,3 linkages reveals that the accommodation of the glucosyl unit in subsite +1 (Asn639) is indeed split between two different binding modes: the proper orientation leading to α-1,6 glucosylation is ensured by Trp675 (subsite +2), whereas the orientation leading to α-1,3 glucosylation is controlled by Asp772 (subsite +2′), assisted by Trp543 (subsite +3′). As such, subsite +1 does not control linkage specificity and rather appears to be "undecided" with regard to the linkage promiscuity of ASR. It is the positioning of the glucosyl unit in subsite +2 or +2′ that determines linkage specificity and eventually resolve the ASR linkage hesitation, as previously proposed by Moulis et al.[14] It can be assumed that the mechanism will operate during the synthesis of longer oligosaccharides as the enzyme catalytic cleft will only "see" the last 2 or 3 glucosyl units of the growing chain. If we extrapolate this for the synthesis of an HMM alternan, the "round-trip" mechanism between the two sites would result in an accumulation of alternating α-1,6 and α-1,3 linkages in the polymer, with the only variable being the number of consecutive α-1,6 linkages. This not only is in accordance with the α-1,6/α-1,3 ratio observed in the HMM alternan (roughly 2:1) but also corroborates the fact that linkage alternation is kinetically determined.[49]

CONCLUSION

We disclosed herein the first crystal structure of ASR from *L. citreum* NRRL B-1355, the largest structure of a glucansucrase solved so far. Structural analysis showed that the enzyme is stabilized thanks to its calcium binding site and an entire domain V. In addition, the presence of longer loops in domain A and extended hydrophobic packing in domain C have been identified as traits specific to ASR that could influence the enhanced enzyme's stability. Concerning catalytic activity, we showed that domain V participates in polymer elongation, especially to produce HMM alternan. Focusing on the catalytic core of the enzyme, we selected several mutation targets and discerned their effect on alternan or oligoalternans formation using a combination of acceptor reaction and HPLC/MS. Combining these data with molecular docking and structural analysis, we identified two different acceptor subsites, +2 and +2′, that are specific to the synthesis of α-1,6 and α-1,3 linkages, respectively. Our data set allowed us to propose the mechanism by which the ASR catalytic cleft differentiates the incoming acceptors based on the nature of the terminal glucosidic linkage. This mechanism leads to the formation of alternate α-1,3 or α-1,6 linkages in the alternan polymer. Our results shed new light on a long known but very interesting enzyme that could pave the way for further engineering efforts with the aim of producing tailor-made α-glucan polysaccharides.

ASSOCIATED CONTENT

Supporting Information

The Supporting Information is available free of charge on the ACS Publications website at DOI: 10.1021/acscatal.8b04510.

DOI: 10.1021/acscatal.8b04510
ACS Catal. 2019, 9, 2222−2237

Primers used in the study, acceptor reaction chromatograms, data collection on the crystal, NMR of truncated mutant products, DSF profiles, mass spectrum, views and comparison of domain C and domain V, view of the catalytic site with subsites −1 and +1, docking with α-1,3 branching glucosylation (PDF)

AUTHOR INFORMATION

Corresponding Authors

*E-mail: cioci@insa-toulouse.fr.
*E-mail: remaud@insa-toulouse.fr.

ORCID

Magali Remaud-Siméon: 0000-0002-2658-672X

Notes

The authors declare no competing financial interest.

ACKNOWLEDGMENTS

We are grateful to MetaSys, the Metabolomics & Fluxomics Center at the Laboratory of Biological Systems and Process Engineering (Toulouse, France), for the NMR experiments. Our special thanks go to the European Synchrotron Radiation Facility (ESRF, Grenoble, France) and the Structural Biophysics team of the Institute of Pharmacology and Structural Biology (IPBS, Toulouse, France) for access to the crystallization facility and help in synchrotron data collection. We thank the ICEO facility, which is part of the Integrated Screening Platform of Toulouse (PICT), for providing access to HPLC and protein purification equipment. We are very grateful to Florent Grimaud for his technical assistance.

ABBREVIATIONS

ASR, alternansucrase; HMM, high molar mass; LMM, low molar mass; GH, glycoside-hydrolase; GS, glucansucrase; DP, degree of polymerization; OD, oligodextran; OA, oligoalternan; TSS, transition state stabilizer; IM2, isomaltose; IM3, isomaltotriose

REFERENCES

(1) Badel, S.; Bernardi, T.; Michaud, P. New Perspectives for Lactobacilli Exopolysaccharides. *Biotechnol. Adv.* **2011**, *29*, 54−66.
(2) Suresh Kumar, A.; Mody, K.; Jha, B. Bacterial Exopolysaccharides − a Perception. *J. Basic Microbiol.* **2007**, *47*, 103−117.
(3) Monsan, P.; Bozonnet, S.; Albenne, C.; Joucla, G.; Willemot, R.-M.; Remaud-Siméon, M. Homopolysaccharides from Lactic Acid Bacteria. *Int. Dairy J.* **2001**, *11*, 675−685.
(4) Naessens, M.; Cerdobbel, A.; Soetaert, W.; Vandamme, E. J. Leuconostoc Dextransucrase and Dextran: Production, Properties and Applications. *J. Chem. Technol. Biotechnol.* **2005**, *80*, 845−860.
(5) Bounaix, M.-S.; Gabriel, V.; Robert, H.; Morel, S.; Remaud-Siméon, M.; Gabriel, B.; Fontagné-Faucher, C. Characterization of Glucan-Producing Leuconostoc Strains Isolated from Sourdough. *Int. J. Food Microbiol.* **2010**, *144*, 1−9.
(6) Jeanes, A.; Haynes, W. C.; Wilham, C. A.; Rankin, J. C.; Melvin, E. H.; Austin, M. J.; Cluskey, J. E.; Fisher, B. E.; Tsuchiya, H. M.; Rist, C. E. Characterization and Classification of Dextrans from Ninety-Six Strains of Bacteria. *J. Am. Chem. Soc.* **1954**, *76*, 5041−5052.
(7) Côté, G. L.; Robyt, J. F. Isolation and Partial Characterization of an Extracellular Glucansucrase from *Leuconostoc Mesenteroides* NRRL B-1355 That Synthesizes an Alternating (1→6),(1→3)-α-D-Glucan. *Carbohydr. Res.* **1982**, *101*, 57−74.
(8) Dertli, E.; Colquhoun, I. J.; Côté, G. L.; Le Gall, G.; Narbad, A. Structural Analysis of the α-d-Glucan Produced by the Sourdough Isolate *Lactobacillus Brevis* E25. *Food Chem.* **2018**, *242*, 45−52.
(9) Goldstein, I. J.; Whelan, W. J. 32. Structural Studies of Dextrans. Part I. A Dextran Containing α-1, 3-Glucosidic Linkages. *J. Chem. Soc.* **1962**, *0*, 170−175.
(10) Hare, M. D.; Svensson, S.; Walker, G. J. Characterization of the Extracellular, Water-Insoluble α-D-Glucans of Oral Streptococci by Methylation Analysis, and by Enzymic Synthesis and Degradation. *Carbohydr. Res.* **1978**, *66*, 245−264.
(11) Joucla, G.; Pizzut, S.; Monsan, P.; Remaud-Siméon, M. Construction of a Fully Active Truncated Alternansucrase Partially Deleted of Its Carboxy-Terminal Domain. *FEBS Lett.* **2006**, *580*, 763−768.
(12) Leathers, T. D.; Nunnally, M. S.; Côté, G. L. Modification of Alternan by Dextranase. *Biotechnol. Lett.* **2009**, *31*, 289−293.
(13) Misaki, A.; Torii, M.; Sawai, T.; Goldstein, I. J. Structure of the Dextran of *Leuconostoc Mesenteroides* B-1355. *Carbohydr. Res.* **1980**, *84*, 273−285.
(14) Moulis, C.; Joucla, G.; Harrison, D.; Fabre, E.; Potocki-Veronese, G.; Monsan, P.; Remaud-Siméon, M. Understanding the Polymerization Mechanism of Glycoside-Hydrolase Family 70 Glucansucrases. *J. Biol. Chem.* **2006**, *281*, 31254−31267.
(15) Seymour, F. R.; Knapp, R. D.; Chen, E. C. M.; Bishop, S. H.; Jeanes, A. Structural Analysis of Leuconostoc Dextrans Containing 3-O-α-D-Glucosylated α-D-Glucosyl Residues in Both Linear-Chain and Branch-Point Positions, or Only in Branch-Point Positions, by Methylation and by 13C-N.M.R. Spectroscopy. *Carbohydr. Res.* **1979**, *74*, 41−62.
(16) Seymour, F. R.; Knapp, R. D.; Bishop, S. H. Correlation of the Structure of Dextrans to Their 1H-N.M.R. Spectra. *Carbohydr. Res.* **1979**, *74*, 77−92.
(17) Seymour, F. R.; Slodki, M. E.; Plattner, R. D.; Jeanes, A. Six Unusual Dextrans: Methylation Structural Analysis by Combined g.l.c.—m.s. of per-O-Acetyl-Aldononitriles. *Carbohydr. Res.* **1977**, *53*, 153−166.
(18) Seymour, F. R.; Knapp, R. D.; Bishop, S. H. Determination of the Structure of Dextran by 13C-Nuclear Magnetic Resonance Spectroscopy. *Carbohydr. Res.* **1976**, *51*, 179−194.
(19) Torii, M.; Sakakibara, K. Column Chromatographic Separation and Quantitation of α-Linked Glucose Oligosaccharides. *J. Chromatogr. A* **1974**, *96*, 255−257.
(20) López-Munguía, A.; Pelenc, V.; Remaud, M.; Biton, J.; Michel, J. M.; Lang, C.; Paul, F.; Monsan, P. Production and Purification of Alternansucrase, a Glucosyltransferase from *Leuconostoc Mesenteroides* NRRL B-1355, for the Synthesis of Oligoalternans. *Enzyme Microb. Technol.* **1993**, *15*, 77−85.
(21) López Munguía, A.; Pelenc, V.; Remaud, M.; Paul, F.; Monsan, P.; Biton, J.; Michel, J. M.; Lang, C. Production and Purification of *Leuconostoc Mesenteroides* NRRL B-1355 Alternansucrase. *Ann. N. Y. Acad. Sci.* **1990**, *613*, 717−722.
(22) Argüello-Morales, M. A.; Remaud-Siméon, M.; Pizzut, S.; Sarçabal, P.; Willemot, R.-M.; Monsan, P. Sequence Analysis of the Gene Encoding Alternansucrase, a Sucrose Glucosyltransferase from *Leuconostoc Mesenteroides* NRRL B-1355. *FEMS Microbiol. Lett.* **2000**, *182*, 81−85.
(23) Wangpaiboon, K.; Padungros, P.; Nakapong, S.; Charoenwongpaiboon, T.; Rejzek, M.; Field, R. A.; Pichyangkura, R. An α-1,6-and α-1,3-Linked Glucan Produced by *Leuconostoc Citreum* ABK-1 Alternansucrase with Nanoparticle and Film-Forming Properties. *Sci. Rep.* **2018**, *8*, 8340.
(24) Côté, G. L. Low-Viscosity α-d-Glucan Fractions Derived from Sucrose Which Are Resistant to Enzymatic Digestion. *Carbohydr. Polym.* **1992**, *19*, 249−252.
(25) Argüello Morales, M. A.; Remaud-Siméon, M.; Willemot, R.-M.; Vignon, M. R.; Monsan, P. Novel Oligosaccharides Synthesized from Sucrose Donor and Cellobiose Acceptor by Alternansucrase. *Carbohydr. Res.* **2001**, *331*, 403−411.
(26) Côté, G. L.; Holt, S. M.; Miller-Fosmore, C. Prebiotic Oligosaccharides via Alternansucrase Acceptor Reactions. In *Oligosaccharides in Food and Agriculture*; ACS Symposium Series;

DOI: 10.1021/acscatal.8b04510
ACS Catal. 2019, 9, 2222−2237

American Chemical Society: Washington, DC, 2003; Vol. *849*, pp 76−89.
(27) Holt, S. M.; Miller Fosmore, C. M.; Côté, G. L. Growth of Various Intestinal Bacteria on Alternansucrase-Derived Oligosaccharides. *Lett. Appl. Microbiol.* **2005**, *40*, 385−390.
(28) Sanz, M. L.; Côté, G. L.; Gibson, G. R.; Rastall, R. A. Prebiotic Properties of Alternansucrase Maltose-Acceptor Oligosaccharides. *J. Agric. Food Chem.* **2005**, *53*, 5911−5916.
(29) Musa, A.; Miao, M.; Zhang, T.; Jiang, B. Biotransformation of Stevioside by *Leuconostoc Citreum* SK24.002 Alternansucrase Acceptor Reaction. *Food Chem.* **2014**, *146*, 23−29.
(30) Grimaud, F.; Faucard, P.; Tarquis, L.; Pizzut-Serin, S.; Roblin, P.; Morel, S.; Le Gall, S.; Falourd, X.; Rolland-Sabaté, A.; Lourdin, D.; Moulis, C.; Remaud-Siméon, M.; Potocki-Veronese, G. Enzymatic Synthesis of Polysaccharide-Based Copolymers. *Green Chem.* **2018**, *20*, 4012−4022.
(31) Janeček, S.; Svensson, B.; Russell, R. R. Location of Repeat Elements in Glucansucrases of Leuconostoc and Streptococcus Species. *FEMS Microbiol. Lett.* **2000**, *192*, 53−57.
(32) Joucla, G. Caractérisation de l'alternane-saccharase de *Leuconostoc mesenteroides* NRRL B-1355 : Approche rationnelle et aléatoire pour la conception de nouvelles glucane-saccharases. Thèse de doctorat, Institut National Des Sciences Appliquées de Toulouse: Toulouse, 2003.
(33) Petersen, T. N.; Brunak, S.; von Heijne, G.; Nielsen, H. SignalP 4.0: Discriminating Signal Peptides from Transmembrane Regions. *Nat. Methods* **2011**, *8*, 785−786.
(34) Linding, R.; Jensen, L. J.; Diella, F.; Bork, P.; Gibson, T. J.; Russell, R. B. Protein Disorder Prediction: Implications for Structural Proteomics. *Structure* **2003**, *11*, 1453−1459.
(35) Yang, Z. R.; Thomson, R.; McNeil, P.; Esnouf, R. M. RONN: The Bio-Basis Function Neural Network Technique Applied to the Detection of Natively Disordered Regions in Proteins. *Bioinformatics* **2005**, *21*, 3369−3376.
(36) Buchan, D. W. A.; Minneci, F.; Nugent, T. C. O.; Bryson, K.; Jones, D. T. Scalable Web Services for the PSIPRED Protein Analysis Workbench. *Nucleic Acids Res.* **2013**, *41*, W349−357.
(37) Studier, F. W. Protein Production by Auto-Induction in High Density Shaking Cultures. *Protein Expression Purif.* **2005**, *41*, 207−234.
(38) Miller, G. L. Use of Dinitrosalicylic Acid Reagent for Determination of Reducing Sugar. *Anal. Chem.* **1959**, *31*, 426−428.
(39) Côté, G. L.; Robyt, J. F. Acceptor Reactions of Alternansucrase from *Leuconostoc Mesenteroides* NRRL B-1355. *Carbohydr. Res.* **1982**, *111*, 127−142.
(40) Côté, G. L.; Sheng, S. Penta-, Hexa-, and Heptasaccharide Acceptor Products of Alternansucrase. *Carbohydr. Res.* **2006**, *341*, 2066−2072.
(41) Kabsch, W. XDS. *Acta Crystallogr., Sect. D: Biol. Crystallogr.* **2010**, *66*, 125−132.
(42) Winn, M. D.; Ballard, C. C.; Cowtan, K. D.; Dodson, E. J.; Emsley, P.; Evans, P. R.; Keegan, R. M.; Krissinel, E. B.; Leslie, A. G. W.; McCoy, A.; McNicholas, S. J.; Murshudov, G. N.; Pannu, N. S.; Potterton, E. A.; Powell, H. R.; Read, R. J.; Vagin, A.; Wilson, K. S. Overview of the CCP4 Suite and Current Developments. *Acta Crystallogr., Sect. D: Biol. Crystallogr.* **2011**, *67*, 235−242.
(43) Murshudov, G. N.; Skubák, P.; Lebedev, A. A.; Pannu, N. S.; Steiner, R. A.; Nicholls, R. A.; Winn, M. D.; Long, F.; Vagin, A. A. REFMAC5 for the Refinement of Macromolecular Crystal Structures. *Acta Crystallogr., Sect. D: Biol. Crystallogr.* **2011**, *67*, 355−367.
(44) Vriend, G. WHAT IF: A Molecular Modeling and Drug Design Program. *J. Mol. Graphics* **1990**, *8*, 52−56.
(45) Chen, V. B.; Arendall, W. B.; Headd, J. J.; Keedy, D. A.; Immormino, R. M.; Kapral, G. J.; Murray, L. W.; Richardson, J. S.; Richardson, D. C. MolProbity: All-Atom Structure Validation for Macromolecular Crystallography. *Acta Crystallogr., Sect. D: Biol. Crystallogr.* **2010**, *66*, 12−21.
(46) Piovesan, D.; Minervini, G.; Tosatto, S. C. E. The RING 2.0 Web Server for High Quality Residue Interaction Networks. *Nucleic Acids Res.* **2016**, *44*, W367−W374.
(47) Nivedha, A. K.; Thieker, D. F.; Makeneni, S.; Hu, H.; Woods, R. J. Vina-Carb: Improving Glycosidic Angles during Carbohydrate Docking. *J. Chem. Theory Comput.* **2016**, *12*, 892−901.
(48) Claverie, M.; Cioci, G.; Vuillemin, M.; Monties, N.; Roblin, P.; Lippens, G.; Remaud-Siméon, M.; Moulis, C. Investigations on the Determinants Responsible for Low Molar Mass Dextran Formation by DSR-M Dextransucrase. *ACS Catal.* **2017**, *7*, 7106−7119.
(49) Côté, G. L.; Sheng, S.; Dunlap, C. A. Alternansucrase Acceptor Products. *Biocatal. Biotransform.* **2008**, *26*, 161−168.
(50) Ito, K.; Ito, S.; Shimamura, T.; Weyand, S.; Kawarasaki, Y.; Misaka, T.; Abe, K.; Kobayashi, T.; Cameron, A. D.; Iwata, S. Crystal Structure of Glucansucrase from the Dental Caries Pathogen *Streptococcus Mutans*. *J. Mol. Biol.* **2011**, *408*, 177−186.
(51) Pijning, T.; Vujičić Žagar, A.; Kralj, S.; Dijkhuizen, L.; Dijkstra, B. W. Flexibility of Truncated and Full-Length Glucansucrase GTF180 Enzymes from *Lactobacillus Reuteri* 180. *FEBS J.* **2014**, *281*, 2159−2171.
(52) Brison, Y.; Malbert, Y.; Czaplicki, G.; Mourey, L.; Remaud-Siméon, M.; Tranier, S. Structural Insights into the Carbohydrate Binding Ability of an α-(1→2) Branching Sucrase from Glycoside Hydrolase Family 70. *J. Biol. Chem.* **2016**, *291*, 7527−7540.
(53) Vujičić-Žagar, A.; Pijning, T.; Kralj, S.; López, C. A.; Eeuwema, W.; Dijkhuizen, L.; Dijkstra, B. W. Crystal Structure of a 117 KDa Glucansucrase Fragment Provides Insight into Evolution and Product Specificity of GH70 Enzymes. *Proc. Natl. Acad. Sci. U. S. A.* **2010**, *107*, 21406−21411.
(54) MacGregor, E. A.; Jespersen, H. M.; Svensson, B. A Circularly Permuted α-Amylase-Type α/β-Barrel Structure in Glucan-Synthesizing Glucosyltransferases. *FEBS Lett.* **1996**, *378*, 263−266.
(55) Davies, G. J.; Wilson, K. S.; Henrissat, B. Nomenclature for Sugar-Binding Subsites in Glycosyl Hydrolases. *Biochem. J.* **1997**, *321*, 557−559.
(56) Robert, X.; Gouet, P. Deciphering Key Features in Protein Structures with the New ENDscript Server. *Nucleic Acids Res.* **2014**, *42*, W320−W324.
(57) Nagi, A. D.; Regan, L. An Inverse Correlation between Loop Length and Stability in a Four-Helix-Bundle Protein. *Folding Des.* **1997**, *2*, 67−75.
(58) Meng, X.; Pijning, T.; Tietema, M.; Dobruchowska, J. M.; Yin, H.; Gerwig, G. J.; Kralj, S.; Dijkhuizen, L. Characterization of the Glucansucrase GTF180 W1065 Mutant Enzymes Producing Polysaccharides and Oligosaccharides with Altered Linkage Composition. *Food Chem.* **2017**, *217*, 81−90.
(59) Monchois, V.; Vignon, M.; Russell, R. R. B. Mutagenesis of Asp-569 of Glucosyltransferase I Glucansucrase Modulates Glucan and Oligosaccharide Synthesis. *Appl. Environ. Microbiol.* **2000**, *66*, 1923−1927.
(60) Shimamura, A.; Nakano, Y. J.; Mukasa, H.; Kuramitsu, H. K. Identification of Amino Acid Residues in *Streptococcus Mutans* Glucosyltransferases Influencing the Structure of the Glucan Product. *J. Bacteriol.* **1994**, *176*, 4845−4850.
(61) Meng, X.; Dobruchowska, J. M.; Pijning, T.; López, C. A.; Kamerling, J. P.; Dijkhuizen, L. Residue Leu940 Has a Crucial Role in the Linkage and Reaction Specificity of the Glucansucrase GTF180 of the Probiotic Bacterium *Lactobacillus Reuteri* 180. *J. Biol. Chem.* **2014**, *289*, 32773−32782.

DOI: 10.1021/acscatal.8b04510
ACS Catal. 2019, 9, 2222−2237